remote sensing

MDPI

Article

Characterization of CYGNSS Ocean Surface Wind Speed Products

Christopher Ruf [1,*], Mohammad Al-Khaldi [2], Shakeel Asharaf [3], Rajeswari Balasubramaniam [1], Darren McKague [1], Daniel Pascual [4], Anthony Russel [1], Dorina Twigg [1] and April Warnock [5]

1 Space Physics Research Laboratory, Department of Climate, Space Sciences and Engineering, University of Michigan, Ann Arbor, MI 48109, USA; rajibala@umich.edu (R.B.); dmckague@umich.edu (D.M.); russelan@umich.edu (A.R.); dtwigg@umich.edu (D.T.)
2 ElectroScience Laboratory, Department of Electrical and Computer Engineering, The Ohio State University, Columbus, OH 43210, USA; al-khaldi.2@osu.edu
3 Jet Propulsion Laboratory, University of California, Los Angeles, CA 91330, USA; shakeel.asharaf@jpl.nasa.gov
4 Deimos Space UK Ltd., Didcot OX11 0RL, UK; daniel.pascual@deimos-space.com
5 SRI International, Menlo Park, CA 94025, USA; april.warnock@sri.com
* Correspondence: cruf@umich.edu; Tel.: +1-734-647-0825

Abstract: Since its launch in 2016, a number of wind speed retrieval algorithms have been developed for the NASA CYGNSS satellite observations. We assess their accuracy and precision and characterize the dependence of their performance on environmental factors. The dependence of retrieval uncertainty on the wind speed itself is considered. The triple colocation method of validation is used to correct for the quality of the reference wind speed products with which CYGNSS is compared. The dependence of retrieval performance on sea state is also considered, with particular attention being paid to the long wave portion of the surface roughness spectrum that is less closely coupled to the instantaneous local wind speed than the capillary wave portion of the spectrum. The dependence is found to be significant, and the efficacy of the approaches taken to account for it is examined. The dependence of retrieval accuracy on wind speed persistence (the change in wind speed prior to a measurement) is also characterized and is found to be significant when winds have increased markedly in the ~2 h preceding an observation.

Keywords: ocean surface wind speed; GNSS-R; CYGNSS; bistatic radar

Citation: Ruf, C.; Al-Khaldi, M.; Asharaf, S.; Balasubramaniam, R.; McKague, D.; Pascual, D.; Russel, A.; Twigg, D.; Warnock, A. Characterization of CYGNSS Ocean Surface Wind Speed Products. *Remote Sens.* **2024**, *16*, 4341. https://doi.org/10.3390/rs16224341

Academic Editor: Mark Bourassa

Received: 22 October 2024
Revised: 17 November 2024
Accepted: 19 November 2024
Published: 20 November 2024

1. Introduction

The NASA Cyclone Global Navigation Satellite System (CYGNSS) constellation of eight small satellites was launched on 15 December 2016 into a common circular Earth orbit at ~520 km altitude and 35 deg inclination. Each satellite carries the same Global Navigation Satellite System Reflectometry (GNSS-R) radar receiver, which measures GPS navigation signals reflected by the Earth's surface back into space [1]. The original CYGNSS science objectives were focused on the measurement of near-surface wind speed over the ocean, and early mission validation work reported the uncertainty in those wind speed measurements [2–4]. The scope of the mission has expanded over time to also include GPS reflections over land, from which soil moisture [5], inland water extent [6], and freeze/thaw state [7] can be estimated. The results presented here revisit and expand upon the earlier assessments of ocean wind speed performance. The retrieval algorithm used to produce the standard mission wind speed data product has recently been revised and improved upon, and the latest version is considered here. A new mission wind speed product, optimized for retrieval in major storms (defined as Category 3 or higher, i.e., with a maximum sustained wind speed >49 m/s), is evaluated. The new product also retrieves lower wind speeds as well. The performance of an alternate retrieval algorithm, developed at the NOAA Center

for Satellite Applications and Research, is also assessed. Additional performance characterization tests not previously considered are also included. One is triple colocation validation, which allows for the decomposition of statistical differences between test and reference wind speed estimates into their individual component errors. Another characterization test is included which assesses the performance of wind speed measurements with respect to the persistence of the wind, defined as the change in wind speed in the recent past, prior to the satellite's measurement. This is a new type of performance assessment which has particular relevance to GNSS-R measurements, as discussed in detail below.

2. Materials and Methods

2.1. CYGNSS Wind Speed Data Products

2.1.1. Project v3.2 L2 Fully Developed Seas and L3 Merged Storm Wind Speed

The NASA project science team supporting the CYGNSS mission is responsible for developing, validating, improving, and revising the project data products. These include the Level 1 (L1) calibrated normalized bistatic radar cross section (NBRCS) and slope of the leading edge of the radar return waveform (LES) of the ocean surface [8] and the Level 2 (L2) wind speeds that are retrieved from it. The wind speeds are referenced to a 10 m height above the surface. There are several project wind speed products. The L2 Fully Developed Seas (FDS) wind speed is the general-purpose product that is appropriate for use in conditions other than major organized storms, as described in [9]. In organized cyclonic storm conditions, the sea state tends not to be fully developed, which alters the mapping from wind speed to radar cross section. This is accommodated by adjusting the wind speed retrieval algorithm, as described in [10], to produce the L2 Young Seas Limited Fetch (YSLF) product.

The FDS retrieval algorithm uses empirical geophysical model functions (GMFs) that relate wind speed to NBRCS and LES. The GMFs are derived from a large collection of CYGNSS measurements of NBRCS and LES matched up with near-coincident estimates of the equivalent neutral stability wind speed at 10 m height above the surface produced by the European Centre for Medium Range Weather Forecasting Reanalysis version 5 (ERA5) model. The GMFs are generated using the cumulative distribution function (CDF) matching method, which adjusts the mapping from NBRCS or LES to wind speed so that the resulting distributions of wind speed match that are derived from the population of coincident ERA5 wind speeds [11]. CDF matching is performed separately as a function of incidence angle. The retrieval algorithm inverts the GMF-given NBRCS and LES measurements to estimate the wind speed. The two individual wind speed estimates are then combined using a minimum variance optimal estimator [12]. A secondary correction is made to the retrieved wind speed using a lookup table indexed by the Significant Wave Height (SWH) of the ocean surface estimated by ERA5 at the time of the CYGNSS measurement. The correction accounts for the sensitivity of the measurements to long (swell) wave portions of the ocean surface roughness spectrum that are not directly forced by the local winds. This is in contrast to traditional ocean scatterometer radars, which are only sensitive to the small (capillary) wave portion of the spectrum forced by the local winds. A flowchart description of the retrieval algorithm that generates the FDS and YSLF products is provided in Figure 1a.

The YSLF retrieval algorithm uses the same general approach as FDS with some modifications. An empirical GMF is constructed from near-coincident matchups between CYGNSS measurements of NBRCS and 10 m referenced wind speeds provided by NOAA's Hurricane Weather Research and Forecast system for hurricane prediction (HWRF) reanalysis model. LES measurements are not used because they have a much weaker sensitivity to high winds. HWRF, rather than ERA5, model winds are used as the reference because they are better able to predict the high wind speeds present in major organized storms. The need for a separate GMF in storms results from the fact that the long wave portion of the sea surface roughness spectrum tends to be underdeveloped in organized storms due to the rapidly changing wind speed and direction. As a result, the mapping from wind speed

to NBRCS is significantly different. As with the FDS algorithm, a SWH correction is also made to the YSLF estimate.

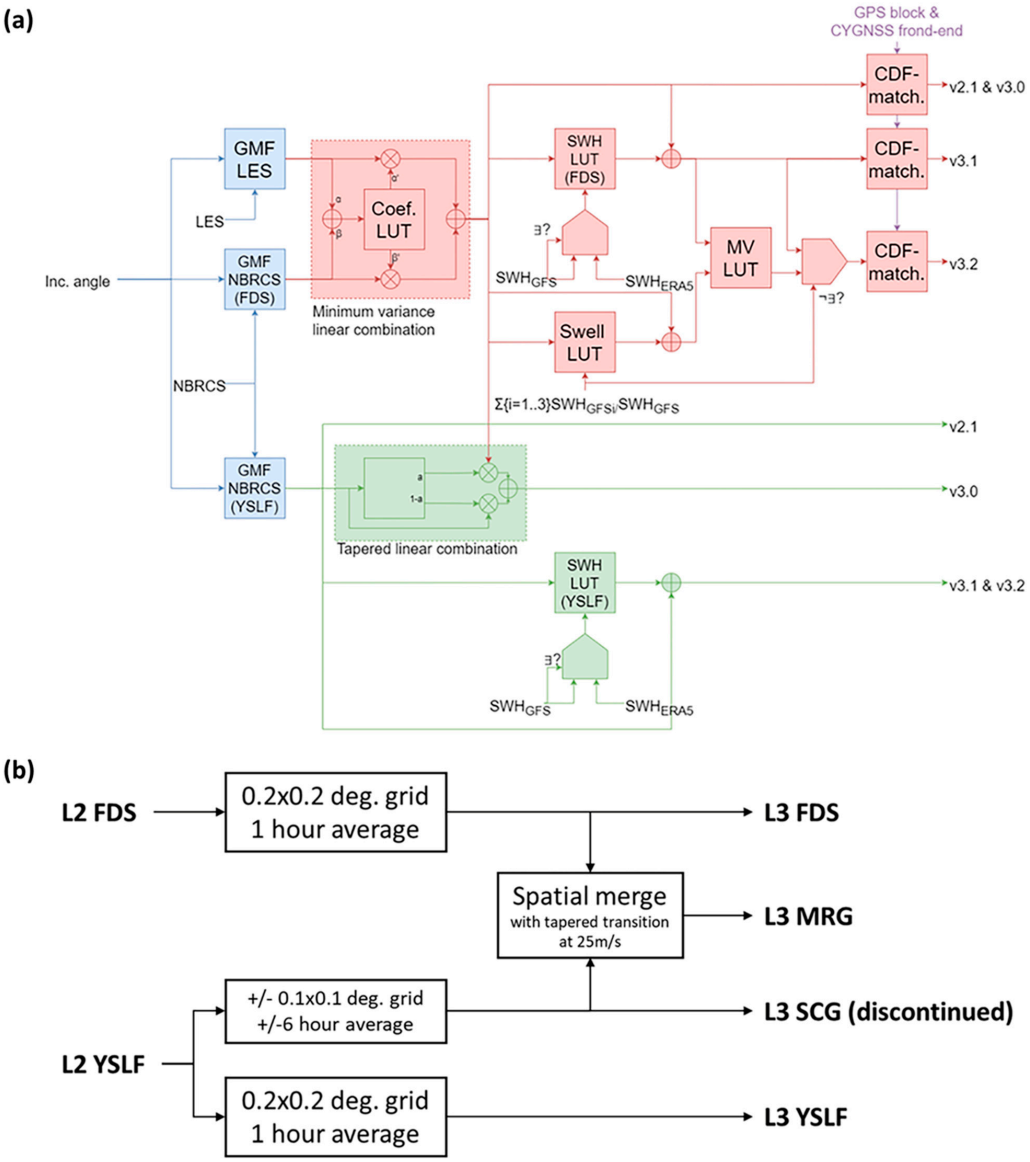

Figure 1. (**a**) Level 2 wind speed processing flow: FDS (maroon) and YSLF (green). (**b**) Level 3 FDS and MRG processing flow.

YSLF is considered an intermediate data product that should not be used indiscriminately due to its limited applicability only in storms. To account for this, a third product, the Level 3 (L3) Merged Storm (MRG) product is provided. MRG combines the YSLF product near storms with the FDS storm away from them. The merging is accomplished using gridded (i.e., Level 3) versions of each to simplify the merging procedure, as described in [13]. A flowchart describing the generation of MRG from FDS and YSLF is shown in Figure 1b.

There have been a number of versions of these products produced over the 7+ years that CYGNSS has been in orbit. The latest version, v3.2, of the FDS and MRG wind speeds is evaluated in this work [14,15].

2.1.2. NOAA v1.2 CYGNSS Wind Speed Product

The NOAA Center for Satellite Applications and Research developed their own CYGNSS wind speed retrieval algorithm and they have produced a data product based on it. There are several differences between their approach and the one used by this project's algorithm, which are summarized here. A more complete description is provided in [16]. L1 calibration of the NBRCS by the project algorithm uses calibration targets on the satellites together with software corrections for the flight hardware behavior [8]. The NOAA algorithm performs a "trackwise correction" to the NBRCS that forces the mean value of the calibrated NBRCS along a specular point track (a ~1000 km long sequence of measurements) to equal the mean NBRCS predicted by passing ERA5 wind speed values through a CYGNSS forward model that predicts NBRCS from wind. Trackwise correction forces better agreement between satellite observations and model winds at the expense of some loss in their independence. NOAA's algorithm for wind speed retrieval from NBRCS also uses an empirical GMF derived from near-coincident matchups between NBRCS measurements and reference model winds. In order to account for the differences in NBRCS response to fully developed vs. young sea states, the NOAA matchup dataset from which its GMF is derived consists of ERA5 reference winds at lower wind speeds and HWRF winds at higher wind speeds. This avoids the complication of having multiple wind speed products, which is the case for the project algorithm approach. How well this approach handles high wind retrievals in Fully Developed Sea conditions is one of the performance assessment tests considered below. Another difference with the NOAA approach is the way it handles corrections for SWH, which is to add an additional dimension to their GMF indexed by SWH. This is in contrast to the project algorithm's approach of using a secondary correction table after the GMF conversion from L1 observables to wind speed. Differences between these two approaches with respect to sensitivity to SWH are also examined below. Finally, NOAA's product applies additional spatial averaging to the individual samples using a 25 × 25 km averaging window. Individual samples have a spatial resolution of slightly less than 25 km but there is significant overlap between them, so this type of averaging reduces sample noise significantly while only slightly degrading the spatial resolution.

2.2. Reference Wind Speed Products

2.2.1. Buoys

Surface wind and rain observations from several networks of tropical moored buoy arrays (PIRATA [17], RAMA [18], and TAO/TRITON [19]—see Figure 2) were processed and used as reference data for the CYGNSS wind validation. The validation analysis involves averaging buoy measurements over 60 min intervals and screening them to exclude instances of missing data and data flagged for low quality or sensor failure, which follows the methodology described in [4,20]. The buoy wind speed accuracy is ±0.3 m/s or 3%, with further details available at https://tao.ndbc.noaa.gov/proj_overview/sensors_ndbc.shtml (accessed on 31 January 2024).

Rain gauges are subject to undercatchment errors, particularly in windy conditions. These errors can be substantial, reaching up to 50% at wind speeds of 12 m/s [21]. The data retrieved from the NOAA/PMEL FTP site lack direct corrections for undercatchment. To mitigate this, we employed an approach based on [22] and subsequently by [20], applying a third-order polynomial fit to the dataset to correct for undercatchment in the rain measurements.

Given that CYGNSS winds were reported at a height of 10 m, adjustments were made to buoy wind measurements to align them with this height. The height adjustment was made by applying Monin–Obukhov similarity theory using the COARE (Coupled Ocean-Atmosphere Response Experiment) version 3.6 algorithm, as described by [23,24]. Additionally, buoy wind speeds were converted to equivalent neutral winds to facilitate a direct comparison with the CYGNSS measurements [25].

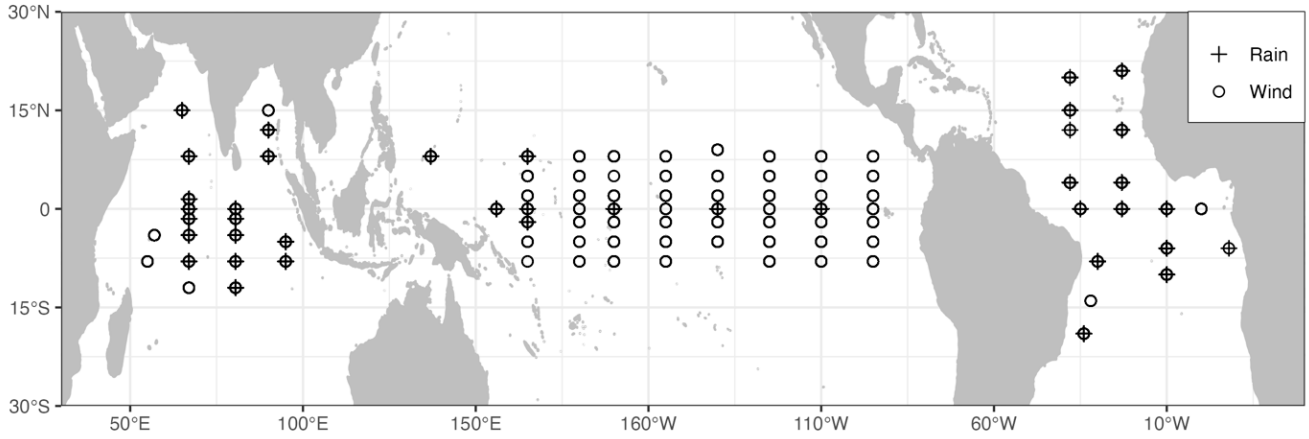

Figure 2. Locations of the colocated tropical buoys used for intercomparison.

In the colocation process, CYGNSS winds were matched within a radius of 25 km and ±30 min of buoy locations and timestamps, using an inverse-distance-weighting (IDW) approach that incorporates both spatial and temporal proximity [4,20,26]. During the matchup process, daily GPS data are utilized to track buoy position over time. A recent observation has identified a notable abrupt temporal instability in the TAO buoy wind time series, characterized by fluctuations of 0.5–0.8 m/s (10%) since mid-2020 [27]. As a result, our buoy CYGNSS verification analysis is limited to observations prior to June 2020. Moreover, the matchups were based on identical sample points between FDS and NOAA to ensure a common set of comparison samples. This results in an aggregated sample size of 21,029 time-space matchup points.

2.2.2. Global Reanalysis Wind Speed Model

Near-coincident matchups were used between CYGNSS observations and ERA5. ERA5 wind speed has been found to have an uncertainty of 1.45 m/s for off-shore winds [28] and an uncertainty of 1.73 m/s globally [29].

The matchup method used with ERA5 initializes a regular grid interpolator object using the modeled data at their associated latitude, longitude, and time. The interpolator takes CYGNSS L2 data dimensioned by latitude, longitude, and time as input and uses trilinear interpolation (nearest neighbor) to estimate ERA5 values at each CYGNSS three-dimensional point. Histograms of the spatial and temporal separation between matchup samples are shown in Figure 3. The mean (±standard deviation) of the distribution of separations is 17.2 km (±15.8 km) and 30.3 min (±16.8 min) for distance and time, respectively. The matchup method for ASCAT-B and GMI (described in Section 2.2.3) starts with all CYGNSS and ERA5 samples within the same hour, then finds the closest matchups to CYGNSS points in lat/lon using a nearest neighbor BallTree algorithm with a Euclidean metric. Only the closest observations in space and within a given time are considered.

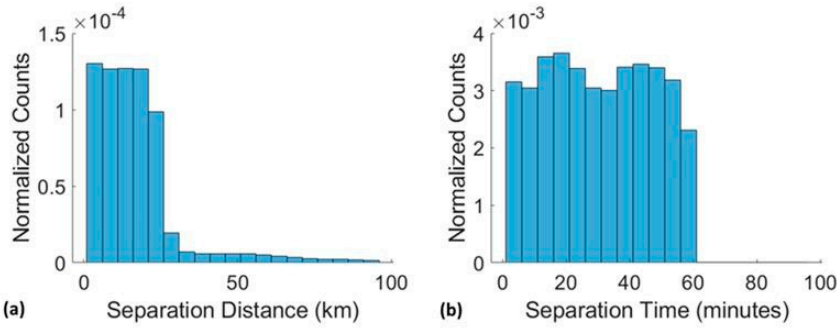

Figure 3. Histograms of (**a**) spatial and (**b**) temporal separation between matchups of CYGNSS and ERA5 wind speed samples. The mean separations are 17.2 km and 30.3 min.

2.2.3. Other Satellite Observations of Winds

Wind speed measurements made by two other types of spaceborne microwave sensors are also used for intercomparison purposes. One is the ASCAT-B scatterometer flying on the Metop-B satellite. ASCAT-B is a backscatter radar that operates at C-Band with VV polarization and its operation is optimized for ocean wind observations [30]. The second spaceborne sensor is the GMI microwave radiometer flying on the Global Precipitation Measurement satellite. GMI is a multi-frequency/multi-polarization microwave radiometer designed to measure both atmospheric and surface geophysical parameters, including near-surface wind speed over ocean [31]. Notably, these two wind sensors rely on different remote sensing modalities and frequencies (radar backscatter at C-Band and passive microwave emission at X-, Ku-, K-, and Ka-Band) than CYGNSS (forward specular scatter at L-Band) to measure the wind speed, so their respective measurement errors and their sensitivity to ancillary geophysical parameters can be expected to be largely uncorrelated.

2.2.4. Storm Winds

The CYGNSS MRG and NOAA wind speed products over most major hurricanes during 2018–2022 were matched up with two reference ocean surface wind products, with measurements being made by the Stepped Frequency Microwave Radiometer (SFMR) and HWRF reanalysis model winds. The MRG 34-knot wind radius (R34) product was validated against R34 estimates derived from the ASCAT-B scatterometer described above, the Soil Moisture Active Passive (SMAP) passive microwave radiometer, and Best Track reanalysis storm winds.

SFMR instruments are installed on all U.S. Air Force Reserve Command (AFRC) and NOAA "hurricane hunter" aircraft. SFMR measures the brightness temperature of the ocean surface and atmosphere at six C-band microwave channels, and an overconstrained inversion of the radiative transfer forward model retrieves near surface wind speed and column averaged precipitation. SFMR wind speed uncertainty of 3.9 m/s was estimated from comparisons to coincident dropsonde observations [32]. The version 3 SFMR data product was used in this analysis. SFMR winds were resampled to CYGNSS resolution and were co-located to CYGNSS wind estimates with a maximum temporal separation of 180 min and maximum spatial separation of 0.25 deg lat and lon. The v1.0 SMAP data product was used in this analysis [33]. These data products are L3 daily gridded products with a grid spacing of 0.25 deg. HWRF is an operational model developed by the National Centers for Environmental Prediction. HWRF provides three domains (one parent and two nested) and is based on the initial position of the storm and on the U.S. National Hurricane Center (NHC) forecast of the 72 h storm position. The two nested domains move with the storm with a coverage of 24 deg × 24 deg and 7 deg × 7 deg for the middle and the inner nest, respectively [34]. For our purposes, we used the inner nest gridding, which offers the finest resolution of ~0.015 deg (approx. 2 km). The CYGNSS wind speed estimates are matched to the HWRF inner nest grid, which has a spacing of 2 km. The version 4.0a HWRF winds are re-sampled to CYGNSS resolution and are colocated to CYGNSS wind estimates with a maximum temporal separation of 180 min and a maximum spatial separation of 0.25 deg lat and lon. The Best Track reference wind data come from the NHC's HURDAT2 database [35]. Best Track data were used to assess the performance of the MRG storm product, which is generated at the same 6-hourly cadence as Best Track and uses Best Track to define its storm center location for purposes of storm centric re-gridding.

Two matchup datasets were assembled, one for the MRG winds and another for the NOAA winds, by constraining the different reference dataset measurements to lie within 0.25 deg lat/lon of each other as well as with CYGNSS and within a time window of 180 min. The CYGNSS winds are filtered using several quality measures. Only observations with the overall quality flag set to best quality were used. This resulted in a total dataset consisting of ~1.87 million samples in the MRG-NOAA-SFMR-HWRF dataset. Figure 4 shows the distribution of wind speeds for the two reference and two CYGNSS wind speed products in the matchup dataset. In the figure, the distributions for HWRF and MRG have

more similar high wind tails, which show a lower probability of occurrence than those for SFMR and NOAA. The greater likelihood of high winds with SFMR is probably due to its higher spatial resolution than either HWRF or CYGNSS, which is better able to resolve and detect localized high wind regions of the wind field. The greater occurrence of high wind speeds with NOAA may be due to the hybrid way its GMF was constructed, which tends to overestimate high winds speeds away from the inner core of storms (see Section 3.5 for details).

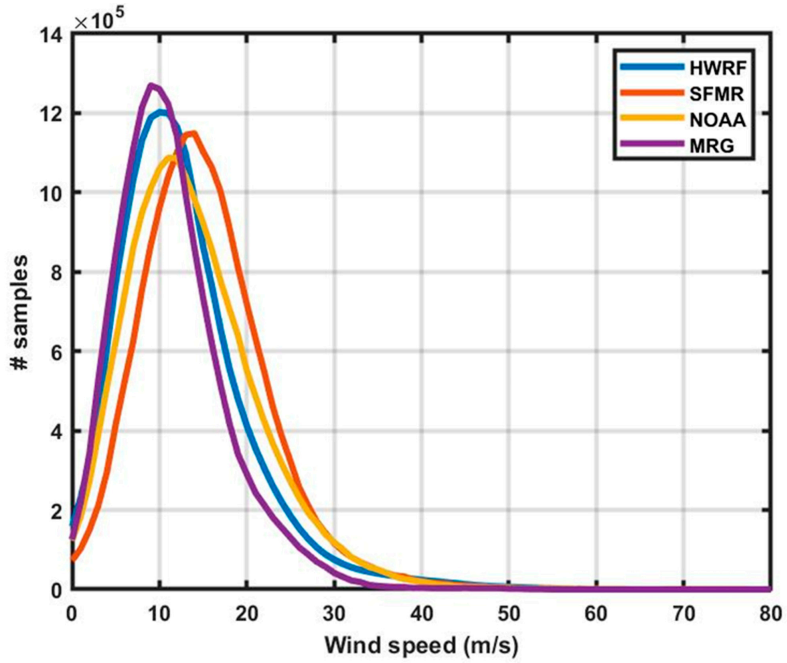

Figure 4. Distribution of the number (#) of data samples in each wind speed bin for the four data products in the storm matchup dataset.

3. Results

The results section contains five types of characterization of the wind speed products: (Section 3.1) Intercomparisons with Reference Wind Speeds; (Section 3.2) Triple Colocation Validation; (Section 3.3) Sampling Properties; (Section 3.4) Sensitivity to Significant Wave Height; and (Section 3.5) Sensitivity to Wind Speed Persistence.

3.1. Intercomparisons with Reference Wind Speeds

3.1.1. Buoy Intercomparison

In this section, comparisons are presented between surface winds measured by CYGNSS and by buoys.

RMSD and Bias Assessment Using Buoys

Figure 5 compares aggregated CYGNSS retrieved surface winds at buoy locations depicted in Figure 2. The retrieved winds closely align with in situ measurements, with correlation coefficients of 0.84 (FDS) and 0.88 (NOAA). However, above ~12 m/s, the collocated CYGNSS samples for both FDS and NOAA exhibit increased dispersion and variability. For FDS, the mean bias is 0.03 m/s, while NOAA winds show a mean bias of −0.22 m/s. These mean biases may result from compensatory effects, where positive biases in low winds counterbalance negative biases in high winds [3]. The Root Mean Square Difference (RMSD) with respect to the buoys is 1.36 m/s (FDS) and 1.21 m/s (NOAA). The trackwise correction and additional spatial averaging applied to NOAA winds may be responsible for its lower RMSD. The RMSD values account for approximately 57% and 50% of the standard deviation of buoy winds in FDS and NOAA, respectively. Given the

tropical buoy wind accuracy of 3% and assuming negligible matchup uncertainty, the upper bounds of CYGNSS retrieval uncertainty for wind speeds (<20 m/s) are approximately 1.33 m/s for FDS and 1.17 m/s for NOAA.

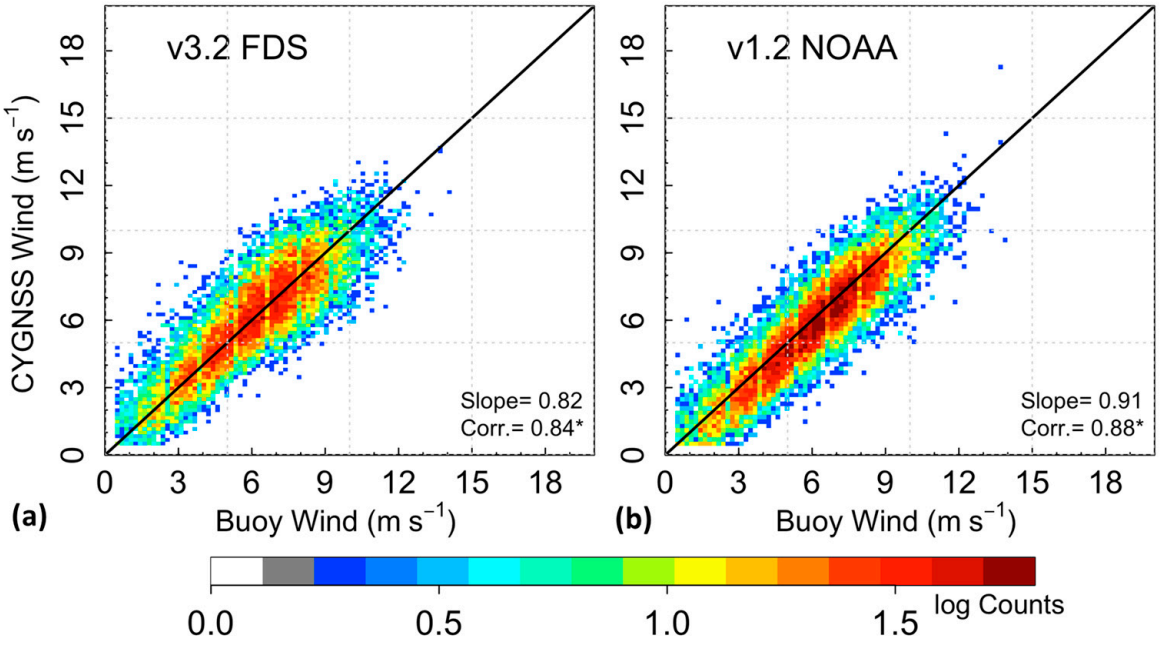

Figure 5. Density scatterplots comparing (**a**) CYGNSS FDS and (**b**) NOAA wind speed products with near-coincident buoy reference winds. 'Slope' represents the best-fit linear regression value, and 'Corr.' denotes its correlation coefficient. Correlation coefficients with a significance level (p-value < 0.05) are marked with an asterisk (*).

Precipitation Dependence

While the influence of rain on the L-band CYGNSS measurements is generally expected to be negligible, intense rainfall conditions may potentially affect the bias and RMSD of CYGNSS wind measurements. To explore the rain effect further, we divide our analysis into two categories based on wind speed (following [4]): ≤6 m/s and >6 m/s. Prior to the rain effect analysis, we eliminate the dependency of CYGNSS residuals on wind following [4].

Figure 6 illustrates the impact of rain on wind residuals at wind speeds below (Figure 5a,b) and above (Figure 6c,d) 6 m/s. The analysis indicates a slight positive bias in CYGNSS measurements at lower wind speeds (Figure 6b), which increases with higher rainfall rates, consistent with prior findings [4,20]. For lower wind speeds, the RMSD values (Figure 6a) in both the CYGNSS products show greater variability during moderate (i.e., R > 0.2 mm/h) and heavy (R > 1.0 mm/h) rain conditions as compared with periods of minimal or no rain (R < 0.1 mm/h). However, the heavy rain scenario also introduces higher sampling uncertainties. The observed positive correlation between precipitation rate and wind RMSD and bias at low wind speeds can be attributed to the anticipated effects of weak diffuse scattering models for winds below approximately 5–6 m/s [36]. Furthermore, the current calibration does not include adjustments for rain-induced signal attenuation [37]. On the other hand, at wind speeds above 6 m/s, the effect of rain on RMSD and bias is relatively low (Figure 6c,d). Note that the NOAA product shows higher error levels than FDS. However, differences in performance between these datasets do not achieve statistical significance.

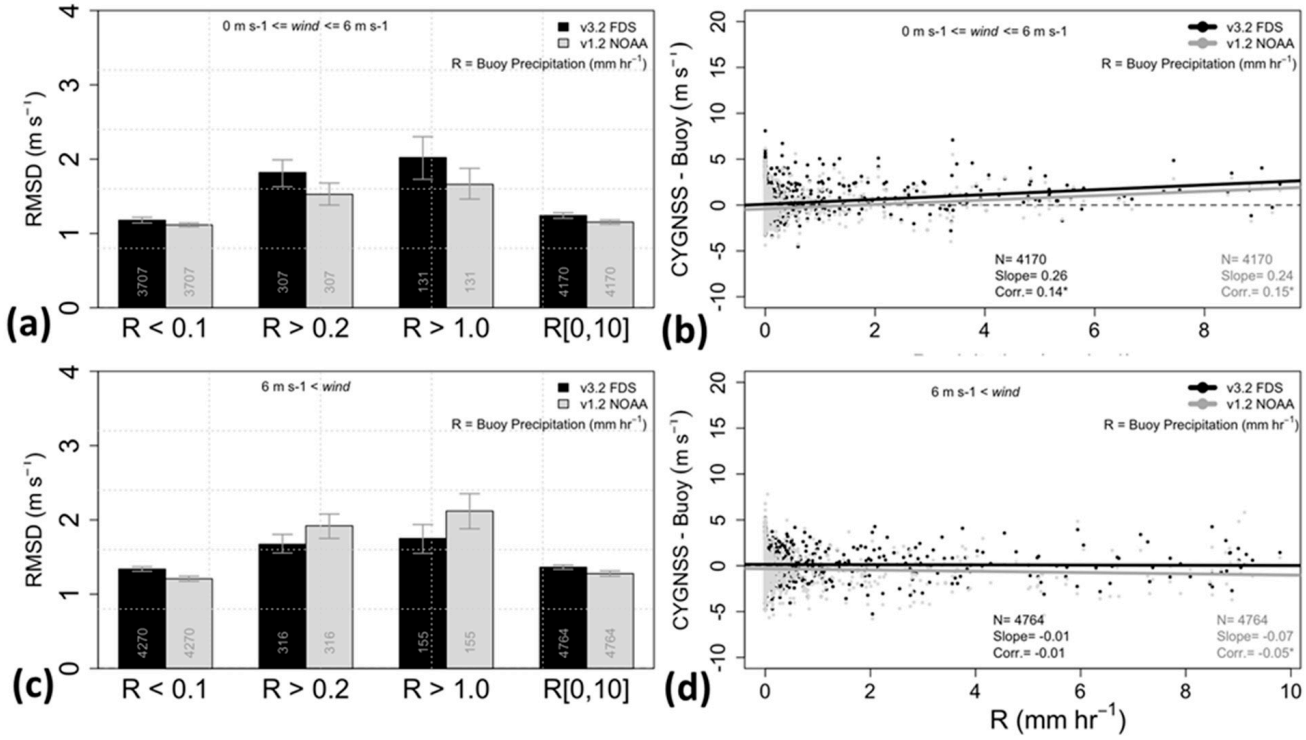

Figure 6. (**a**,**c**) RMSD between CYGNSS and buoys (indicated by bars) at different rain rate (R; in mm/h) conditions, and (**b**,**d**) scatterplot of difference between CYGNSS and buoy winds as functions of buoy precipitation rate, with best-fit linear regression lines overlaid in. Panels (**a**,**b**) correspond to low wind conditions (≤6 m/s), while panels (**c**,**d**) depict conditions with buoy winds >6 m/s. The error bars correspond to the 95% confidence limit estimated via the bootstrap method. Matchup samples are illustrated by the number on each bar. Correlation coefficients with a significance level (p-value < 0.05) are marked with an asterisk (*).

3.1.2. ERA5 Reanalysis Wind Intercomparison

RMSD and Bias Assessment Using ERA5

Figure 7a,b show the comparison between FDS and ERA5. The high-density portion of the scatterplot between FDS and ERA5 (Figure 7a) follows the one-to-one line closely, reflecting the low bias and high correlation between the two. For winds below 20 m/s, the RMSD and bias and the correlation between the FDS and ERA5 winds are 1.6 m/s, 0.1 m/s, and 84%, respectively. Figure 7b shows bias (green) and RMSD (black) as a function of ERA5 wind. For winds between 5 and 7 m/s, which is the peak of the wind distribution shown in blue, the RMSD and bias are approximately 1.4 and 0.3 m/s, respectively. For winds above ~10 m/s, both the bias and RMSD increase in magnitude monotonically, with both estimates beginning to show considerable noise above ~25 m/s due to the small number of samples. Note that differences between FDS and ERA5 winds can result from uncertainties in either product. An attribution of uncertainties to each is discussed in Section 3.2.

Figure 7c,d show comparisons between NOAA and ERA5. The high-density portion of the scatterplot follows the one-to-one line closely from 0 to ~20 m/s, although some outliers with very high NOAA winds appear near 10 m/s. Above 20 m/s, the highest density of NOAA winds tends to be biased high. For winds below 20 m/s, the RMSD, bias, and correlation of the NOAA winds with respect to ERA5 are 1.4 m/s, 0.03 m/s, and 90%, respectively. Figure 7d shows bias (green) and RMSD between the two as a function of ERA5 wind. For winds between 5 and 7 m/s, which is the peak of the wind distribution shown in blue, the RMSD and bias are approximately 1.2 and 0.02 m/s, respectively. For winds above ~10 m/s, both the RMSD and bias increase monotonically up to a peak in both at around 24 m/s, decreasing above this. Differences between NOAA and ERA5 estimates

result from uncertainties in both. Possible causes for the high NOAA bias at high ERA5 wind speeds are discussed in Section 4.

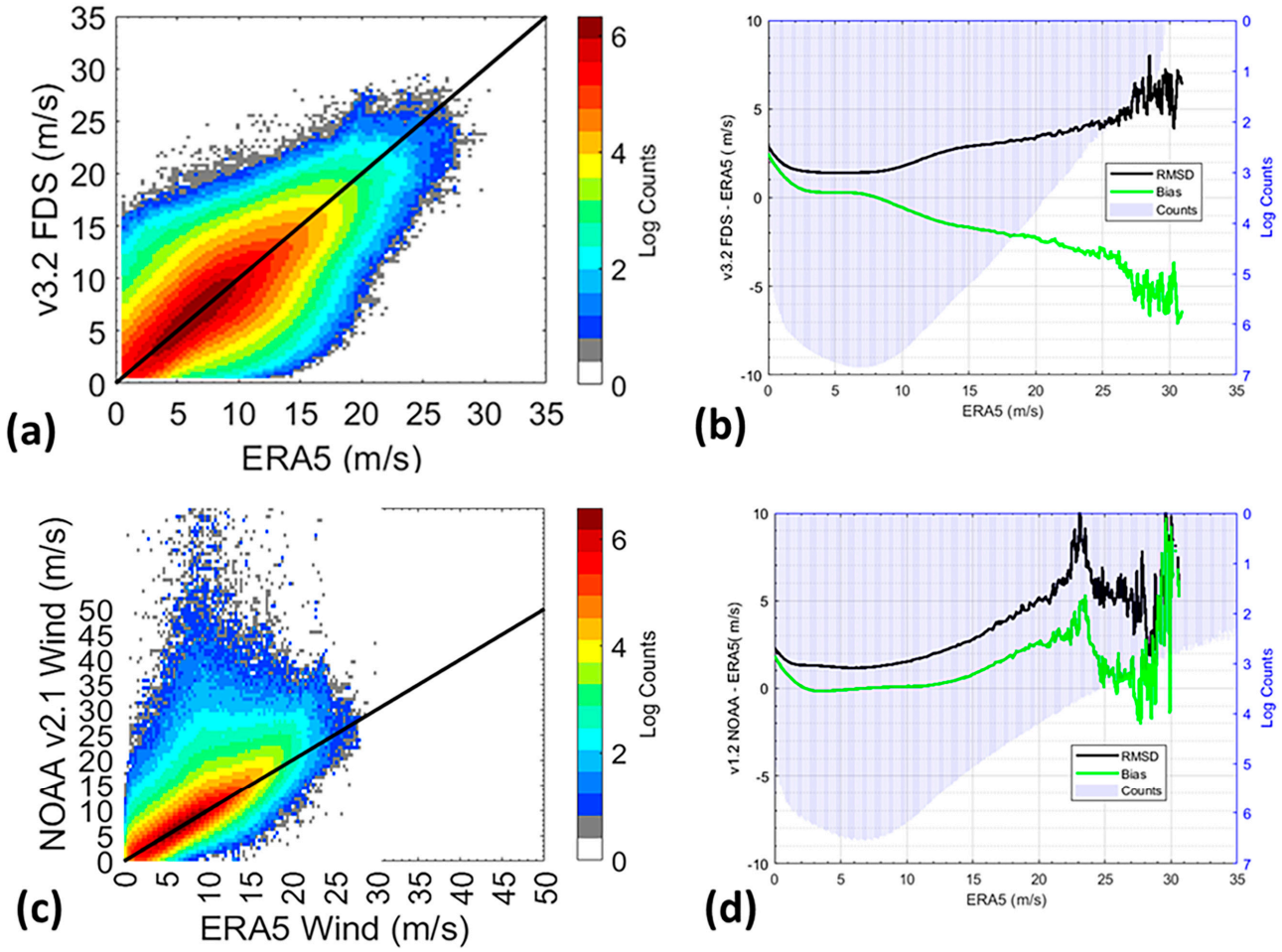

Figure 7. (**a**) Log-density scatterplot between FDS wind speed and ERA5 matchup reference winds. (**b**) RMSD and bias between the two wind speeds as a function of the reference wind. (**c**) Log density scatterplot between NOAA wind speed and ERA5 matchup reference winds. (**d**) RMSD and bias between the two wind speeds as a function of the reference wind. Note the change in scale for (**c**) needed to include NOAA's outliers.

Figure 8 shows a time series of daily FDS vs. ERA5 differences, bias (green) and RMSD (black), from August 2018 to July 2023. Both statistics show roughly periodic oscillations about a consistent mean. For the bias, the time scale of the oscillation is approximately 1 month with a peak-to-peak magnitude of ~0.1 m/s about a mean of −0.2 m/s. For the RMSD, the time scale of the oscillation is approximately 3 months with a peak-to-peak magnitude of ~0.2 m/s about a mean of 1.6 m/s. These time scales are consistent with observed thermal variations in the satellite hardware driven by orbital precession. CYGNSS hardware calibration does include corrections for these temperature dependencies [38], but the small residual oscillations observed in Figure 8 suggest that they have not been fully corrected. A downward trend of ~0.1 m/s is seen in both the bias and RMSD. This may indicate a long-term drift in CYGNSS receivers due to aging but may also result from a drift in ERA5 with respect to the underlying true wind. With both this and the seasonal cycle, it is not possible to definitively determine the root cause.

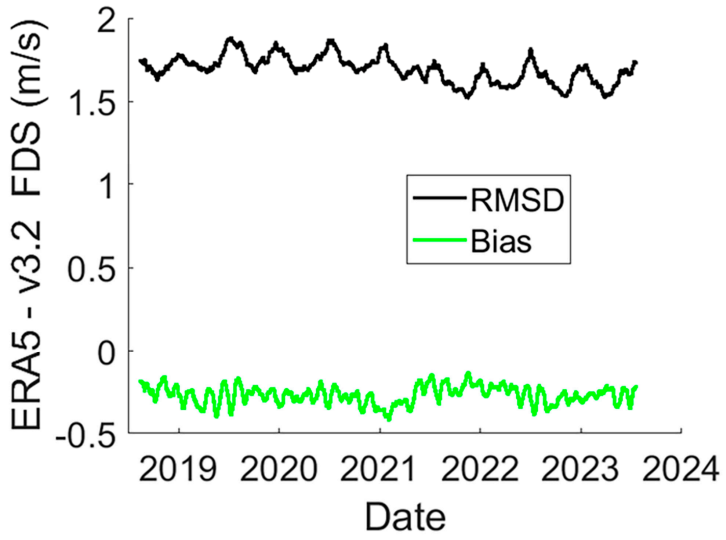

Figure 8. Time series of FDS RMS and mean difference (RMSD and Bias) with respect to ERA5.

Dependence of Performance on GPS and CYGNSS Spacecraft

Figure 9 shows probability distribution functions (PDFs) of the FDS winds separated by a CYGNSS flight model (FM), a CYGNSS antenna (starboard or port), and GPS block type. There is no significant variation in the PDFs between GPS transmitters or CYGNSS receiver hardware, indicating that the hardware calibration algorithms are robust across both CYGNSS and GPS satellites.

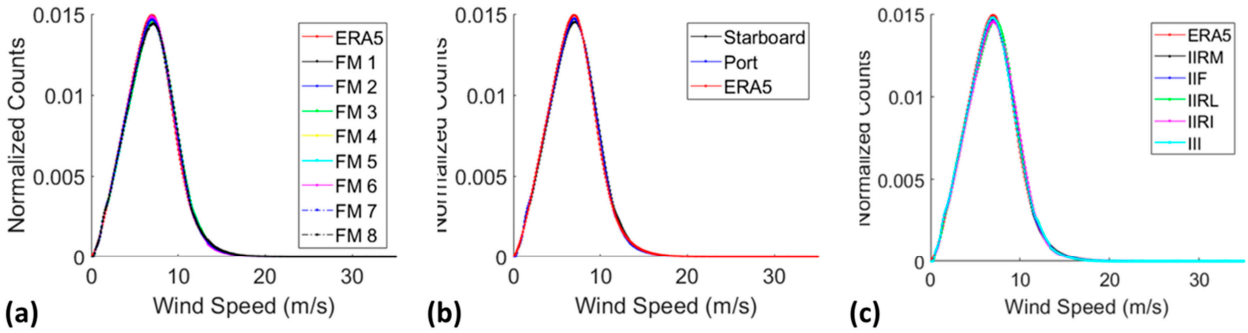

Figure 9. PDFs of v3.2 FDS winds by (**a**) CYGNSS satellite Flight Model (FM), (**b**) port/starboard antenna, and (**c**) GPS block type, with ERA5 winds as the reference.

Geographical Bias Distribution

Figure 10 shows the geographic distribution of FDS bias with respect to ERA5. The figure is derived from a single month of data (December 2023) but is indicative of typical bias distributions throughout the mission. There is a small positive bias in the Intertropical Convergence Zone, likely due to the presence of persistent precipitation (see Section "Precipitation Dependence" for discussion). A previous investigation addressed the impact of precipitation on GNSS-R ocean observations and found that both splash-induced surface roughening and the outflow of downdrafts caused by rain can introduce wind speed retrieval biases [37]. Other isolated regions of biases can be seen that may be due to radio frequency interference (RFI) from supplemental navigation sources. For example, the high bias seen in the Mediterranean is at a geometry consistent with the location of one of the geostationary satellites in the Indian Space Research Organization's NavIC constellation. Similar characterizations were noted in a 2019 study [39]. However, the RFI environment can be quite dynamic and may have changed in the intervening time.

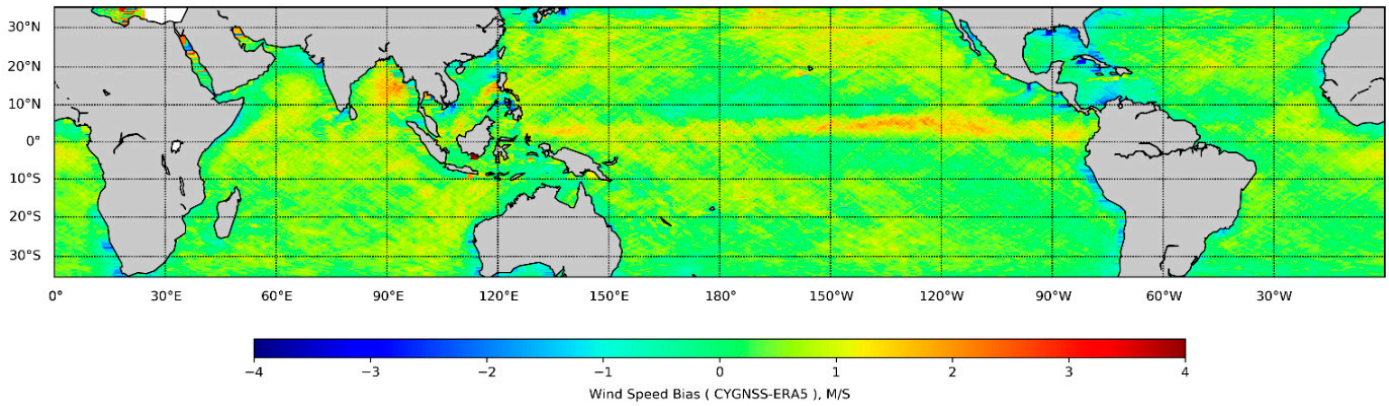

Figure 10. Geographical distribution of FDS bias with respect to ERA5 (FDS—ERA5). Data are averaged over all of December 2023.

3.2. Triple Colocation Validation

Triple colocation is a powerful means of assessing the performance of remotely sensed environmental parameters when they are compared with other near-coincident estimates of the same parameter. It attempts to decompose the differences between the two into individual components of error due to each of them. In order to apply the method, it is necessary to assemble near-coincident estimates of the environmental parameter from three different sources. These matchup "triplets" provide an overconstrained system of equations for the parameters of their joint probability distribution, from which the individual distributions can be factored [40]. Decomposition of the joint distribution is only possible if the errors in each of the three estimates are mutually uncorrelated. If this is not the case, the triple colocation results may be inaccurate. This possibility is addressed by assembling more than three near-coincident matchups and then performing the triple colocation analysis on all possible triplets. If the sources are sufficiently different (e.g., predictions by different models or measurements by different types of sensors), then the degree and type of mutual correlation between their errors can be expected to differ, and the validity of the resulting triple colocation analysis likewise to differ. However, if the results are found to be similar, this is an indication that the effects of mutually correlated error may not be significant. In the following applications of the triple colocation method, we assemble four or more matchup sources and compare the results derived from all possible triplets taken from among them.

Triple colocation performance assessment is performed separately for storm and non-storm conditions. Away from major organized storms, coincident matchups are assembled between the FDS and NOAA CYGNSS winds, the winds measured by ASCAT-B and GMI, and the ERA5 reanalysis winds. For locations in and near major storms, coincident matchups are assembled between the MRG and NOAA CYGNSS winds, the winds measured by SFMR, and the HWRF model winds. Note that with both types of matchups, there are more than three available wind speed products to be intercompared.

3.2.1. CYGNSS Global Wind Speed Data Products

The results of the triple colocation analysis for wind speed observations away from storms is summarized in Table 1. Each row of the table considers a different combination of three wind speed products from the five that are available.

The Root Mean Square Error (RMSE) entries are the standard deviations of the error in each of the three products, as estimated by the triple colocation analysis procedure. This results in three different estimates of the RMSE for the two CYGNSS wind speed products (FDS and NOAA) and five different estimates of the RMSE for the three non-CYGNSS products (ERA5, ASCAT, and GMI). Notably, one of the RMSE estimates for the non-CYGNSS products does not involve any CYGNSS data. Since the triple colocation method assumes that the errors in each of the three products are uncorrelated, there will

be some inaccuracies in its estimates of the three RMSE values if here is in fact some correlation. The three non-CYGNSS products were chosen because they use different approaches to determining the wind speed—a reanalysis model, an active backscatter radar, and a passive microwave radiometer—so that their errors can be expected to behave differently and, in particular, their errors will have different correlations with CYGNSS errors and with one another. For this reason, consistency between the RMSE estimates derived using different triplets can be considered an indication that any residual error correlations between products that may be present did not have a significant impact on the RMSE values estimated.

Table 1. Triple colocations results for observations away from storms. Two CYGNSS products and three non-CYGNSS products are used, and various combinations of triplets are considered. The Root Mean Square Error (RMSE) in individual products is estimated for each triplet by the triple colocation analysis procedure.

		RMSE (m/s)				
		FDS	**NOAA**	**ERA5**	**ASCAT**	**GMI**
Triplet of Matchups	FDS, ERA5, ASCAT	1.39	-	0.71	0.42	-
	FDS, ERA5, GMI	1.32	-	0.85	-	0.41
	FDS, ASCAT, GMI	1.34	-	-	0.57	0.31
	NOAA, ERA5, ASCAT	-	1.00	0.66	0.49	-
	NOAA, ERA5, GMI	-	0.93	0.74	-	0.59
	NOAA, ASCAT, GMI	-	1.02	-	0.46	0.45
	ERA5, ASCAT, GMI	-	-	0.76	0.31	0.57
Average RMSE over all triplets		1.35	0.98	0.74	0.45	0.47

The average of the three RMSE estimates for the CYGNSS FDS product is 1.35 m/s and the individual estimates are all within 3% of the average. Similarly, the average RMSE for the CYGNSS NOAA product is 0.98 m/s, with at most 5% deviation between the individual estimates. The lower RMSE for the NOAA product is consistent with earlier results and is believed to result from its use of trackwise correction of the L1 calibration and additional spatial averaging. As an aside, the triple colocation results also provide estimates of the RMSE performance for the three other products, with ASCAT and GMI quite similar at 0.45 and 0.47 m/s and ERA5 slightly higher at 0.74 m/s.

3.2.2. CYGNSS Storm-Specific Data Products

The storm-specific version of the triple colocation analysis uses a similar approach as the non-storm case above, except that the population of wind speeds is divided into bins of different wind speed ranges in order to characterize the performance as a function of wind speed. This is done because the dependence of performance on wind speed becomes significant at higher wind speeds. For consistency of the comparison between the performance of the two CYGNSS products (MRG and NOAA), a matchup dataset simultaneously satisfying the coincidence criteria for all four of MRG, NOAA, SFMR, and HWRF is assembled. This results in a total matchup dataset of 1.87 million samples. Density scatter plots between various pairs of products in the matchup dataset are shown in Figure 11.

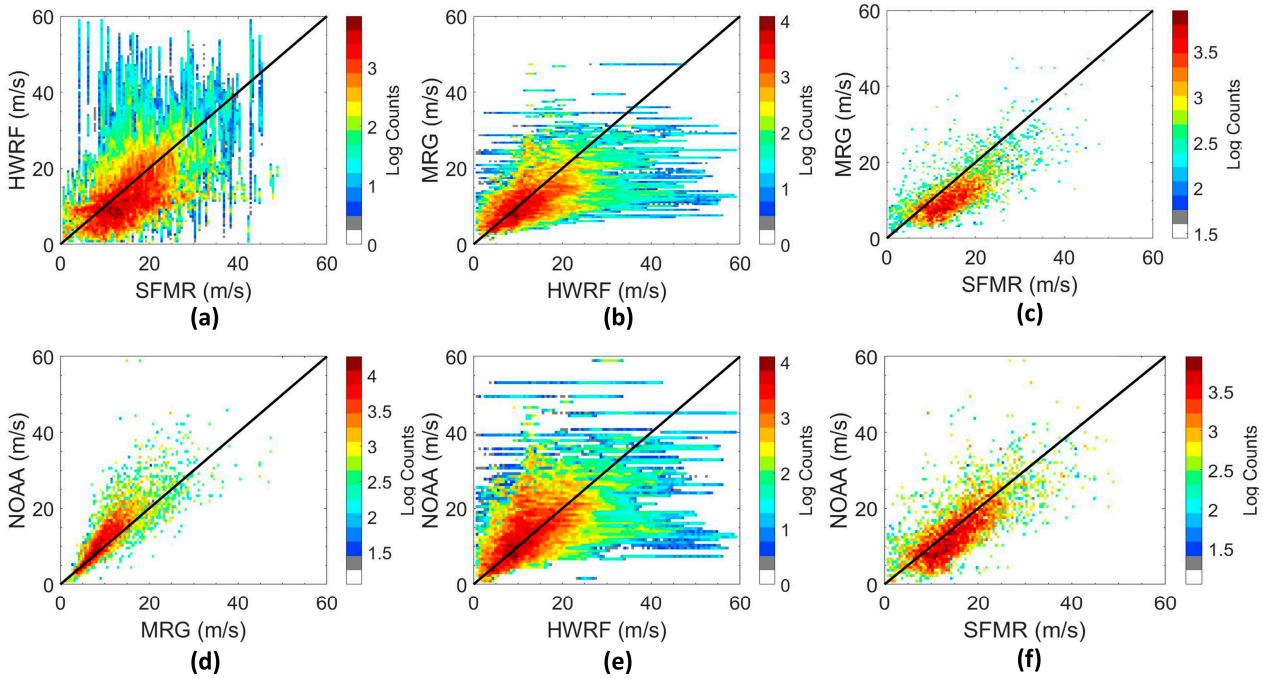

Figure 11. Log density scatterplots for each pair of storm-specific matchup datasets. (**a**) SFMR vs. HWRF, (**b**) HWRF vs. MRG (**c**) SFMR vs. MRG, (**d**) MRG vs. NOAA, (**e**) HWRF vs. NOAA, and (**f**) SFMR vs. NOAA.

Figure 11 highlights the significant increase in scatter that is present when comparisons are made between the HWRF product and any of the other three. This suggests that HWRF has a significantly larger number of outliers than the other products. To address and mitigate this issue, we apply an additional filter to the dataset which requires that matchups are only included if HWRF and SFMR wind speeds differ by less than 10 m/s. The 10 m/s threshold used is an ad hoc value. This reduces the number of samples from ~1.87 million to ~1.64 million in the matchup dataset. The density scatterplots after this filter is applied are shown in Figure 12.

Figure 12a compares HWRF and SFMR and confirms the action of the additional quality filter (compared with Figure 11a). Figure 12b,e plot the MRG and NOAA products against HWRF and show that the most egregious outliers have been removed by the filter. Figure 12c,f plot the MRG and NOAA products against SFMR and demonstrate that their relationships are largely unaffected by the filter—the highest density portion of the dataset is similar to those in Figure 11c,f and the outliers have been largely eliminated. This supports the assertion that HWRF outliers have been largely removed while the relationship of the MRG and NOAA products to SFMR has not been significantly affected. Triple colocation analysis is performed on this filtered matchup dataset.

Table 2 lists the RMSE values derived by triple colocation analysis for the two reference wind speed products. The RMSE values for SFMR are consistent whether MRG or NOAA is used with HWRF to form the triplet of matchups.

SFMR's RMSE values are 2.0–2.3 m/s for wind speeds below 30 m/s and 3–4 m/s above 30 m/s, which is consistent with the results reported in [32]. As expected, HWRF has much larger RMSE values (even after applying the additional filter to remove its most egregious outliers). The RMSE estimates for HWRF are also consistent between the two sets of triplets (HWRF, SFMR, MRG and HWRF, SFMR, NOAA) and they grow with increasing wind speed, from ~3–6 m/s below 30 m/s to ~10 m/s above 30 m/s.

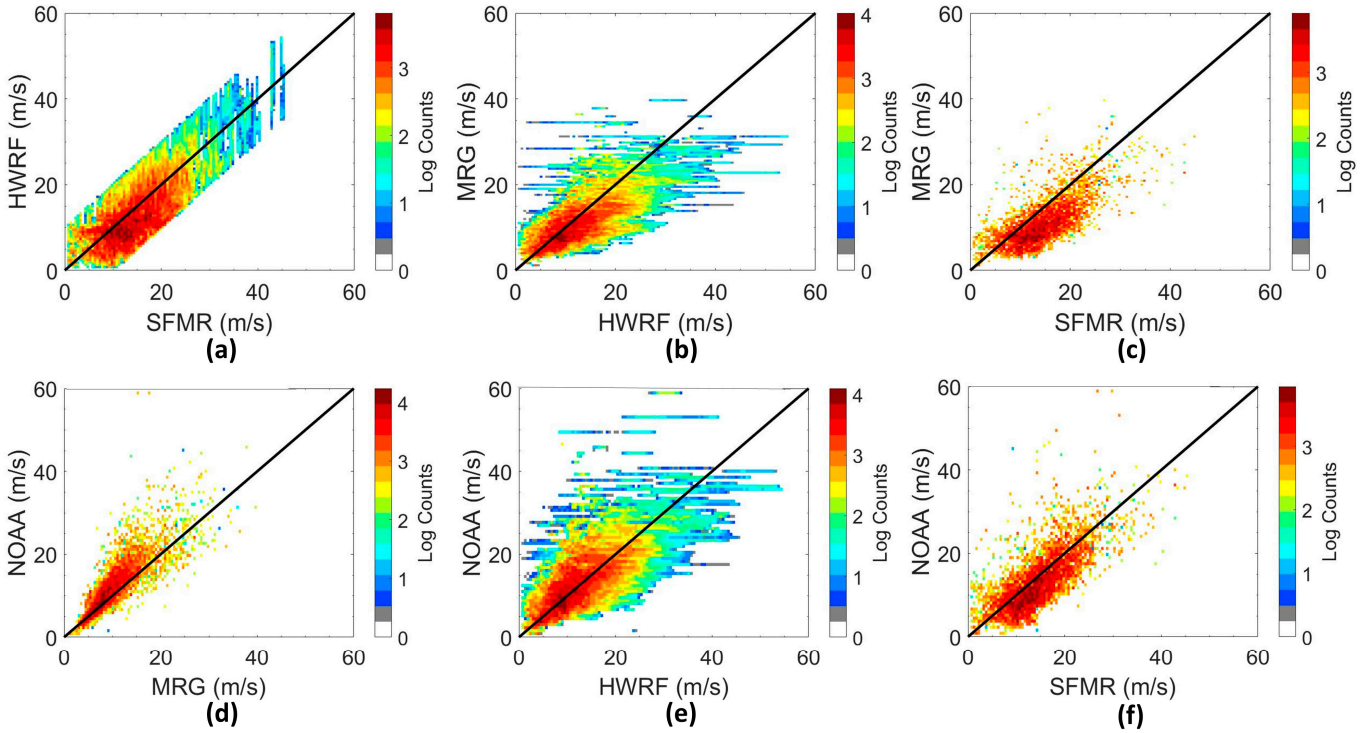

Figure 12. Log density scatterplots after a data-quality filter has been applied which requires coincident HWRF and SFMR values to differ by no more than 10 m/s. (**a**) SFMR vs. HWRF, (**b**) HWRF vs. MRG (**c**) SFMR vs. MRG, (**d**) MRG vs. NOAA, (**e**) HWRF vs. NOAA, and (**f**) SFMR vs. NOAA. These are the samples used for triple colocation analysis.

Table 2. Wind speed bin-wise RMSE of SFMR and HWRF from triple colocation analysis using both CYGNSS high wind speed products, MRG and NOAA.

Reference Wind Speed Product	Triplet of Matchups	Wind Speed Range (m/s)			
		0–10	10–20	20–30	30–75
		RMSE (m/s)			
SFMR	MRG, HWRF, SFMR	2.31	2.20	2.30	2.93
	NOAA, HWRF, SFMR	2.32	1.97	2.19	4.26
HWRF	MRG, HWRF, SFMR	3.77	5.13	6.24	10.17
	NOAA, HWRF, SFMR	3.35	5.37	6.55	10.33

The RMSE of the CYGNSS MRG and NOAA products is estimated in a similar manner using triple colocation except that a finer partitioning of the wind speed is applied in order to better characterize the dependence on wind speed. The results are shown in Figure 13. Also included in the figure is the RMSD between SFMR and each CYGNSS product. The RMSE values for NOAA and MRG are both significantly lower than their RMSD counterparts, with the difference resulting from the error source decomposition performed by the triple colocation analysis. The MRG product has a slightly lower RMSE than the NOAA product, although that difference decreases and they become more comparable at the highest wind speeds.

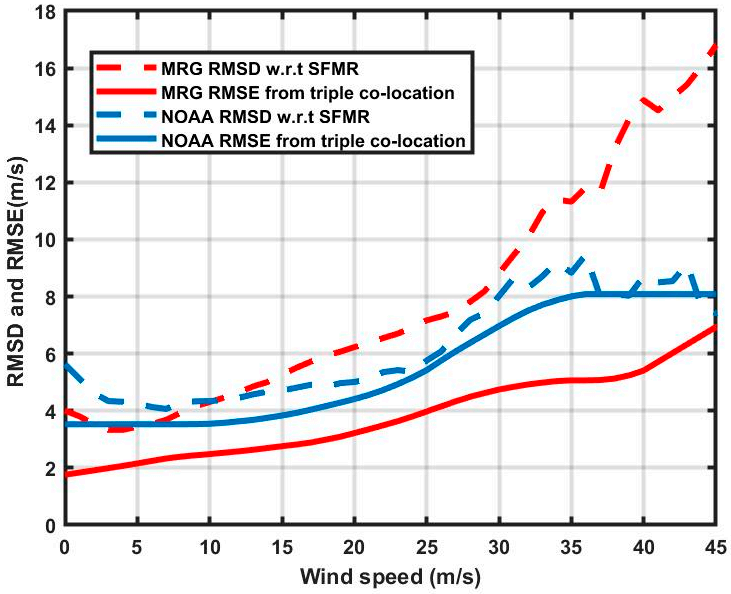

Figure 13. RMSD and RMSE performance for MRG and NOAA products.

34-Knot Significant Wind Radius, R34, in Storms

The CYGNSS MRG wind speed product also produces a secondary product derived from it—the 34-knot wind radius of the storm, R34 [13]. R34 is defined as the minimum distance from the storm center beyond which all wind speeds in a given quadrant are less than 34 knots (~17.5 m/s). It is a metric commonly used by operational agencies to characterize the size of a storm. Uncertainty in the CYGNSS R34 product is also characterized using the triple colocation approach. In this case, the near coincident matchups are between CYGNSS and three other R34 products: (1) estimated directly from wind field measurements made by the spaceborne SMAP passive microwave radiometer; (2) estimated directly from wind field measurements made by the spaceborne ASCAT-B radar scatterometer; and (3) provided by the NOAA Best Track reanalysis model.

The triple colocation results are shown in Table 3. As with previous applications of the method, multiple choices are available to use as triplets and the consistency of the estimated RMSE values for different triplets is an indication of the reliability of the results. The average RMSE value across all three possible triplets is also shown in Table 3. These values, in order from lowest to highest, are 38 km for ASCAT-B, 44 km for Best Track, 49 km for SMAP, and 54 km for CYGNSS. The higher error for CYGNSS, in spite of its relatively low wind speed retrieval error in the vicinity of 34 knots, may be due to the fact that it does not provide a continuous, gap-free image of the storm's wind field. Rather, its measurements are made along narrow tracks as the GPS specular reflection point transits the storm. This spatial undersampling likely results in some gaps in sampling at locations where the wind speed is above and below 34 knots. The somewhat higher CYGNSS errors are in part offset by the more frequent revisit rate of its constellation of satellites (~3 times per day for CYGNSS vs. once every 2–3 days for ASCAT-B and SMAP). The higher revisit rate is also a result of the use of GNSS-R, which lowers the per-satellite cost by approximately two orders of magnitude [6].

A direct scatterplot comparison between CYGNSS and ASCAT-B R34 products is shown in Figure 14 for all quadrants of all the storms included in the matchup dataset. ASCAT-B is chosen as the comparison reference because it has the best (lowest) RMSE measure of performance. The overall bias between the ASCAT-B and CYGNSS R34 products (mean difference across all matchup samples) is only ~2 km. The figure partitions the matchup samples by both storm intensity and quadrant (colors and symbols). The figure demonstrates that CYGNSS R34 performance is fairly consistent as a function of intensity and also between quadrants.

Table 3. Root Mean Square Error (RMSE) in 34-knot significant wind radius (R34) products produced by Best Track (BT), ASCAT-B, SMAP, and CYGNSS MRG. The RMSE in individual products is estimated for each triplet by the triple colocation analysis procedure.

Triplet of Matchups	RMSE (km)			
	BT	ASCAT-B	CYGNSS	SMAP
BT, ASCAT-B, CYGNSS	46.85	36.82	58.33	-
BT, CYGNSS, SMAP	45.57	-	49.47	53.64
BT, ASCAT-B, SMAP	40.05	43.32	-	43.48
ASCAT-B, CYGNSS, SMAP	-	34.73	55.23	48.80
Average RMSE over all triplets	44.2	38.3	54.3	48.6

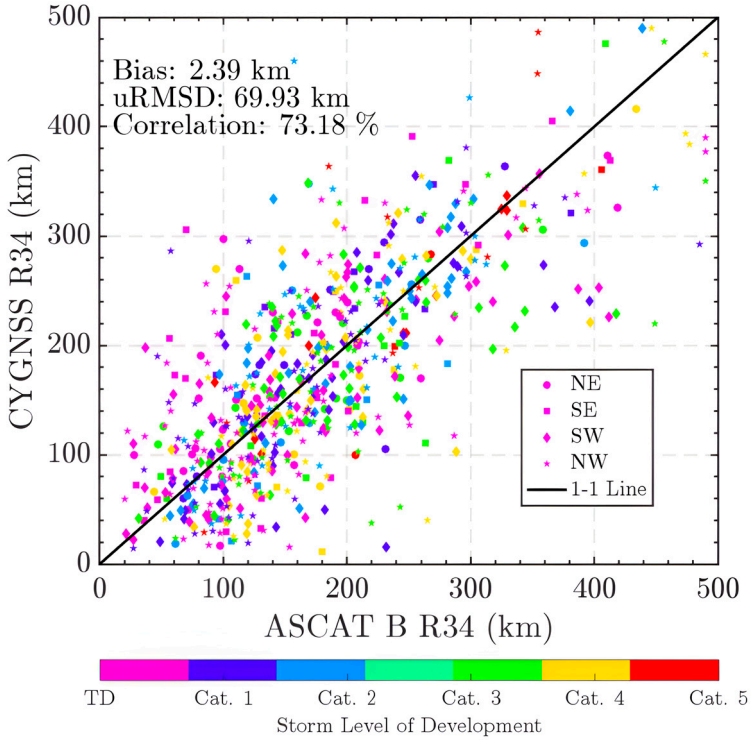

Figure 14. Scatterplot of matchups between the 34-knot wind radius derived from CYGNSS MRG wind fields and those measured by ASCAT. Different storm quadrants are denoted by symbol shapes. Different ranges of storm intensity are denoted by symbol color.

3.3. Sampling Properties

3.3.1. Temporal Sampling of Global Winds

Figure 15 shows the mean revisit time of the CYGNSS FDS wind speed product as a function of latitude, derived from measurements in 2022 but typical of its performance throughout the mission lifetime. Revisit time is defined here as the mean time between measurements within a 72 h time frame for each 0.25° lat, lon box between −35° and 35° latitude that has two or more measurements and 70% spatial coverage. The strong latitudinal dependence seen in the figure results from the 35° orbit inclination of the constellation. Near the equator, the mean revisit time has a maximum of ~4 h. The revisit time decreases to a ~3 h minimum at 35°.

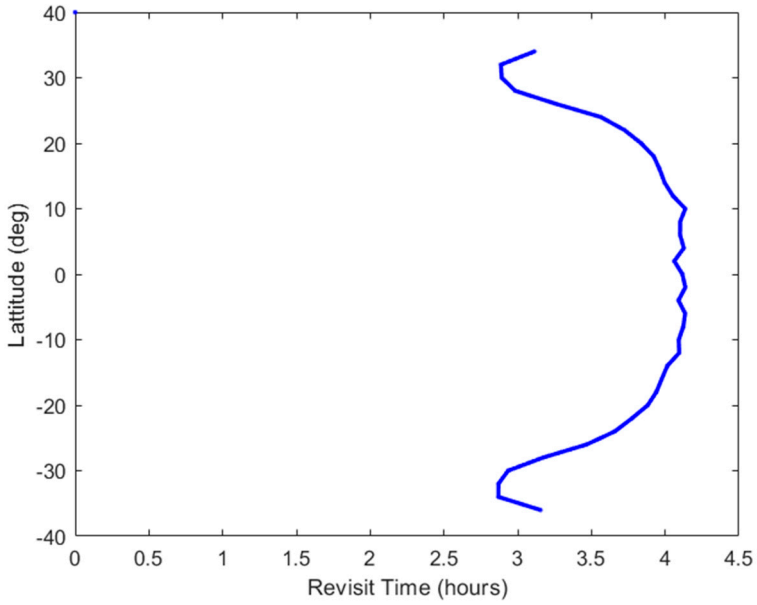

Figure 15. Mean revisit time of FDS wind speed product as a function of latitude.

3.3.2. Sampling of Tropical Cyclone Winds

The MRG product is reported on a 0.1° × 0.1° grid and on a storm-by-storm basis every 6 h from the start to the end of a storm's lifecycle, as defined by Best Track data for storms occurring in the Northern Atlantic and Eastern Pacific basins and by the Joint Typhoon Warning Center (JTWC) for storms occurring in the Western North Pacific, North Indian Ocean, and the Southern Hemisphere basins. Six-hourly reports are only provided if sampling of the storm by the CYGNSS constellation is sufficient.

Table 4 shows the temporal coverage of the MRG product, calculated as the percentage of 6-hourly increments per day that produced wind field reports, averaged over all days throughout the lifecycles of the 360 storms in the dataset covering August 2018–November 2023. The most likely number of reports is three times per day (43%), followed by twice per day (34%), no reports that day (12%), and once per day (11%).

Table 4. Average number of MRG wind fields reported per day from a 360 storm dataset.

Number of reports per day	0	1	2	3	4
% of dataset	12.1	11.1	33.7	42.6	0.52

In addition to wind speed, the MRG product also includes R34 estimates in each storm quadrant, calculated directly from the MRG wind fields. In order to produce an R34 estimate, there must be (1) a crossover from > to <34 knots in the azimuthally averaged radial wind speed profile and (2) sufficient spatial coverage to produce a gap-free radial profile of the wind speed. These conditions are not always met, so R34 estimates are not always available in every quadrant. Table 5 summarizes the frequency of R34 production by specifying what fraction of the time R34 is reported in a given number of quadrants. The table also breaks up R34 production by storm intensity—tropical depression (TD), tropical storm (TS), or typhoons and hurricanes (TY/HU). Table 5 demonstrates that stronger storms tend to have better R34 sampling, with only 3% of wind fields corresponding to TD strength storms producing any R34 values vs. 67% of wind fields corresponding to TY/HU category storms. Among wind fields that report R34 values for at least one quadrant, the wind fields corresponding to TD and TS storm categories are most likely to produce an R34 value for only one quadrant, while wind fields corresponding to TY/HU storm status are most likely to produce R34 values for all four quadrants.

Table 5. R34 MRG temporal and spatial coverage statistics for storms occurring August 2018–November 2023, broken down by the corresponding Best Track storm category of the wind fields.

	TD	TS	TY/HU
Wind fields with no R34 values reported	97%	81%	33%
Wind fields with at least one R34 value reported that report only 1 quadrant	74%	33%	12%
Wind fields with at least one R34 value reported that report 2 quadrants	12%	27%	17%
Wind fields with at least one R34 value reported that report 3 quadrants	9%	15%	16%
Wind fields with at least one R34 value reported that report all 4 quadrants	6%	24%	54%

3.4. Sensitivity to Significant Wave Height

The sensitivity of GNSS-R signals to the long wave portion of the sea state roughness spectrum is discussed in Section 2.1.1. Wind speed retrieval algorithms can attempt to correct for this sensitivity in different ways. With the FDS product, an additive correction is applied after the GMF mapping from Level 1 observables to wind speed using a lookup table that is indexed by the Significant Wave Height (SWH) [41]. With the NOAA product, the GMF itself is indexed by both the L1 observable and the SWH to correct for the sensitivity. The effectiveness of these corrections is examined here. First, to illustrate the importance of the correction, Figure 16a shows a density scatterplot of the error in FDS wind speed vs. SWH if no correction is applied. The error shown is the difference between the FDS wind without its lookup table correction applied and coincident ERA5 matchup wind speeds. In the figure, it can be seen that there is a large positive dispersion of CYGNSS winds at lower SWH values and a large negative bias in the FDS winds at higher SWH values. Figure 16b shows a similar density scatterplot of FDS error after the SWH correction has been applied. Both the low-SWH dispersion and high-SWH bias have been largely mitigated. A similar density scatterplot of the error in the NOAA product is shown in Figure 16c. A small positive dispersion is evident at low SWH values, as is a small positive bias at high SWH values, but both errors are much smaller than those seen in Figure 16a when no correction for SWH has been made.

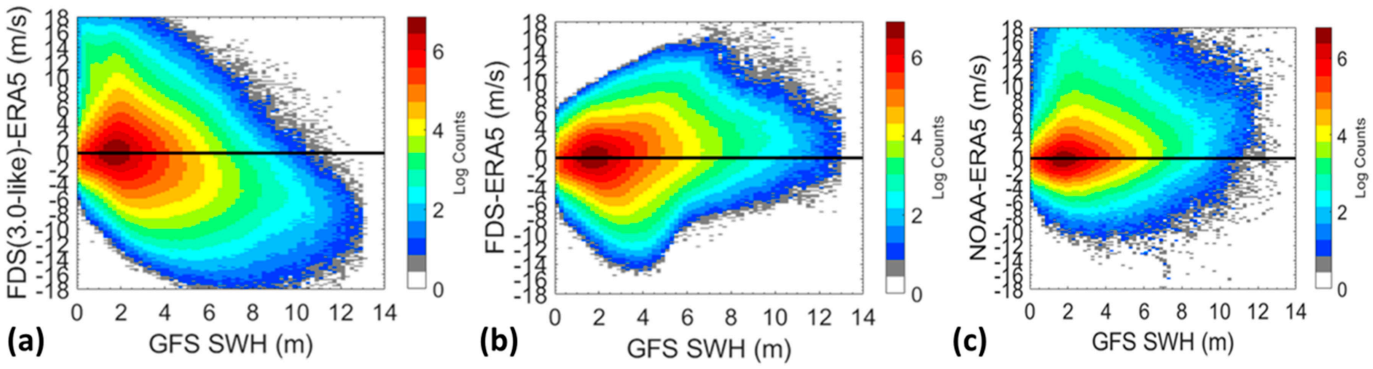

Figure 16. Dependence of CYGNSS wind speed error on SWH: (**a**) FDS without SWH correction, (**b**) FDS with SWH correction, and (**c**) NOAA with SWH correction.

For comparison purposes, the dependence of wind speed error on SWH is shown in Figure 17 for wind products produced by ASCAT-B and GMI. ASCAT-B, a C-band scatterometer, is sensitive only to the capillary wave portion of the surface roughness spectrum, which is largely wind driven. GMI, being a microwave radiometer, is primarily sensitive to the fractional foam coverage on the ocean surface above 7 m/s [31]. In both cases, there

is no significant dependence of the error on SWH. This represents a significant difference between GNSS-R and other remote sensing modalities for wind speed determination.

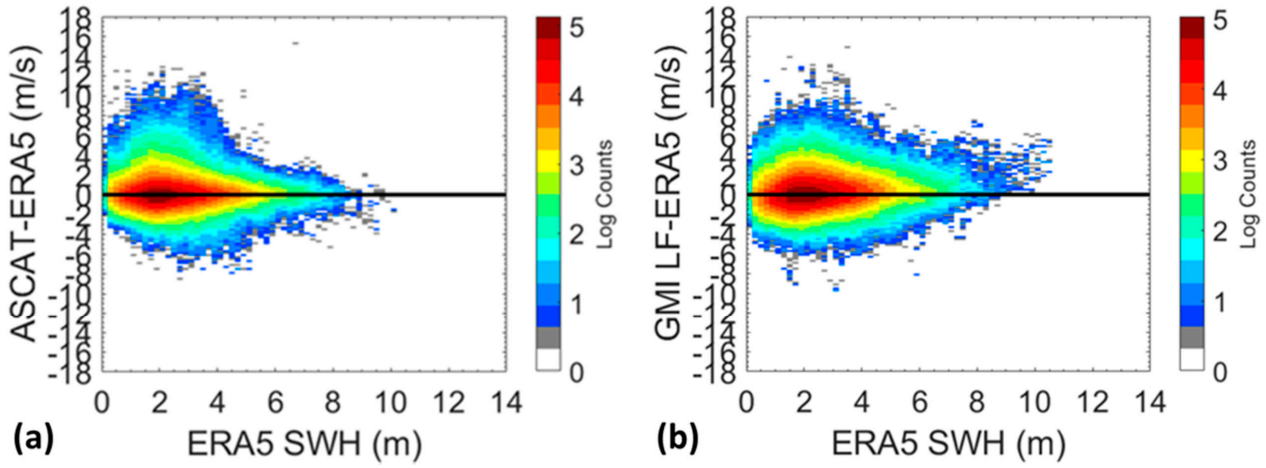

Figure 17. Dependence of (**a**) ASCAT and (**b**) GMI wind speed bias on SWH.

3.5. Sensitivity to Wind Speed Persistence

Stress caused by wind at the ocean surface imparts energy to the surface roughness at capillary-scale wavelengths. Turbulent energy cascade transfers energy from shorter to longer wavelengths and, after a sufficient length of time, the complete roughness spectrum reaches an equilibrium. The equilibrium state is referred to as a Fully Developed Sea. Prior work has shown that the time required for the roughness spectrum to become fully developed with respect to GNSS-R measurements is 1–2 h [42]. In other words, once the wind has blown at the same speed and in the same direction for ~2 h, a GNSS-R measurement will stabilize and the wind speed estimated from it will be consistent with that persistent wind. If, on the other hand, the wind changes in the hours prior to a measurement, the capillary waves will react to the change more quickly than the swell waves and the swell waves at the time of the measurement will not be consistent with the local wind speed. As a result, the wind speed estimated from the measurement may be biased relative to the true wind at the time of the measurement. We consider here the dependence of wind speed bias on wind persistence.

The persistence of wind speed at a given time is a measure of its change in the recent past. For our purposes, we use ERA5 winds reported hourly and define *persistence* at time t as

$$persistence(t) = \frac{windspeed(t) - windspeed(t - 2hr)}{windspeed(t)} \quad (1)$$

where $windspeed(t)$ is the ERA5 wind speed reported at a given time and $windspeed(t - 2\text{ h})$ is the ERA5 wind speed reported at the same location 2 h earlier. We further only considered cases of monotonic change in wind speed between $(t - 2\text{ h})$ and the present, i.e., either $windspeed(t) > windspeed(t - 1\text{ h}) > windspeed(t - 2\text{ h})$ for $persistence > 0$ or $windspeed(t) < windspeed(t - 1\text{ h}) < windspeed(t - 2\text{ h})$ for $persistence < 0$. In practice, monotonicity over 2 h was satisfied in the large majority of cases.

A full year of matchups between CYGNSS and ERA5 winds during 2022 was used for the persistence analysis. The matchups were divided into 5 m/s increments of wind speed (as defined by the CYGNSS wind speed matchup at time, t) and then each increment was further divided by the persistence of the wind speed. The results are shown in Figure 18 for the FDS wind product.

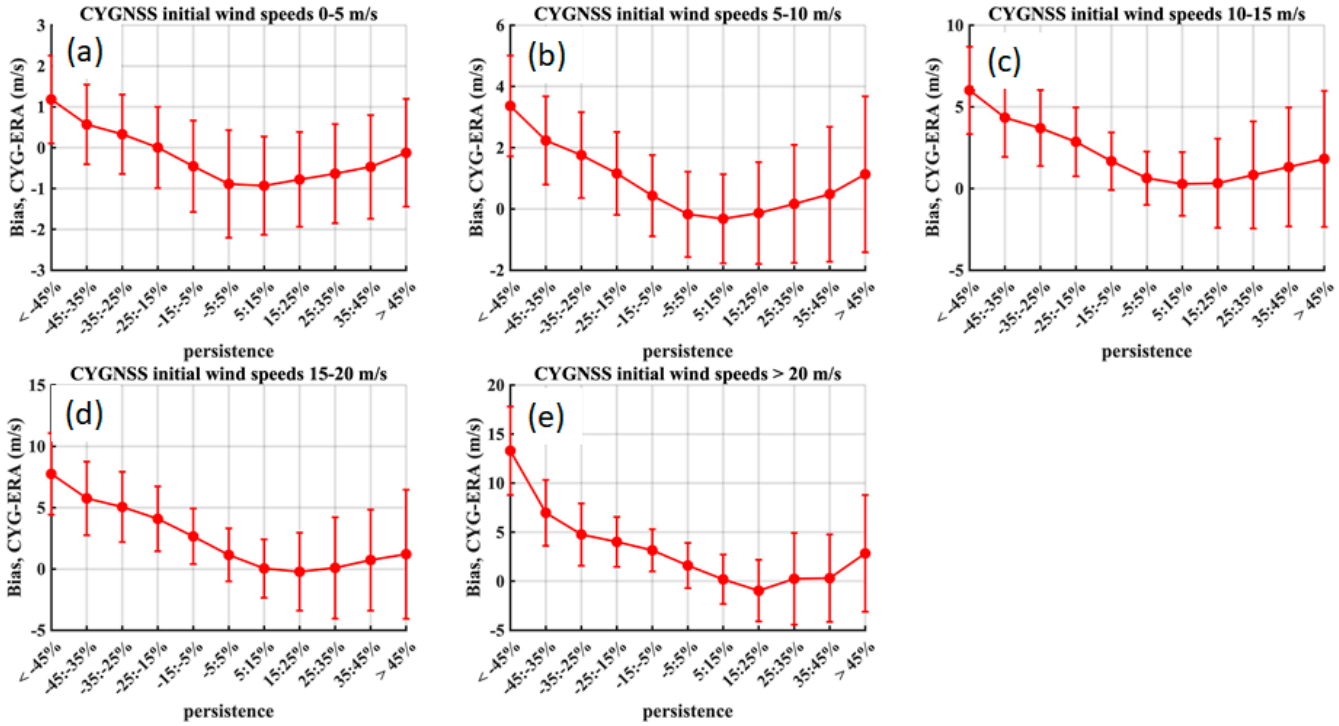

Figure 18. Bias in the CYGNSS FDS wind speed product as a function wind speed persistence for wind speed ranges of (**a**) 0–5 m/s, (**b**) 5–10 m/s, (**c**) 10–15 m/s, (**d**) 15–20 m/s, (**e**) >20 m/s. Persistence < 0 implies prior winds were higher. Bias is the average (FDS–ERA5) difference for all of CY2022. Error bars are the standard deviation of all samples averaged in each wind speed and persistence bin.

For each wind speed interval, the bias (mean difference between CYGNSS and ERA5) is shown as a function of persistence. Error bars are included to show the standard deviation of the population of samples averaged in each case. Several characteristics apparent in Figure 18 are noteworthy. For all wind speeds above 5 m/s, the bias is within ±0.5 m/s of zero when the persistence is small (between −15% and +15%). For larger positive values of persistence, in which case the prior wind speed was significantly lower than the present wind, there is a small increase in the bias. More notably, for large negative values of persistence, the bias grows dramatically with increasing persistence. These are cases in which the prior wind was significantly higher than the present wind. The explanation of this result is that the longer wave portion of the roughness spectrum is still responding to the higher winds that were there in the past. This increases the overall roughness and decreases the NBRCS. The retrieval algorithm therefore overestimates the wind speed, resulting in a large positive bias (FDS >> ERA5).

Figure 19 shows persistence results for the NOAA wind speed product relative to ERA5. Below 15 m/s, the dependence of bias on persistence was similar to that of the FDS product. Above 15 m/s, the relative change in bias with persistence was similar but there is a significant overall positive bias in the NOAA product for all values of persistence. NOAA consistently overestimates the wind speed for winds above 15 m/s, with a bias of ~3–5 m/s at winds speeds of 15–20 m/s and a bias of ~10 m/s at wind speeds > 20 m/s. Also note the very large standard deviation of individual bias values at wind speeds > 20 m/s. Both of these characteristics (high mean bias and large variations in individual bias) are believed to be due to the fact that the high wind portion of the NOAA GMF has been tuned to tropical cyclone conditions, which tend to have very different surface roughness spectra than do Fully Developed Seas.

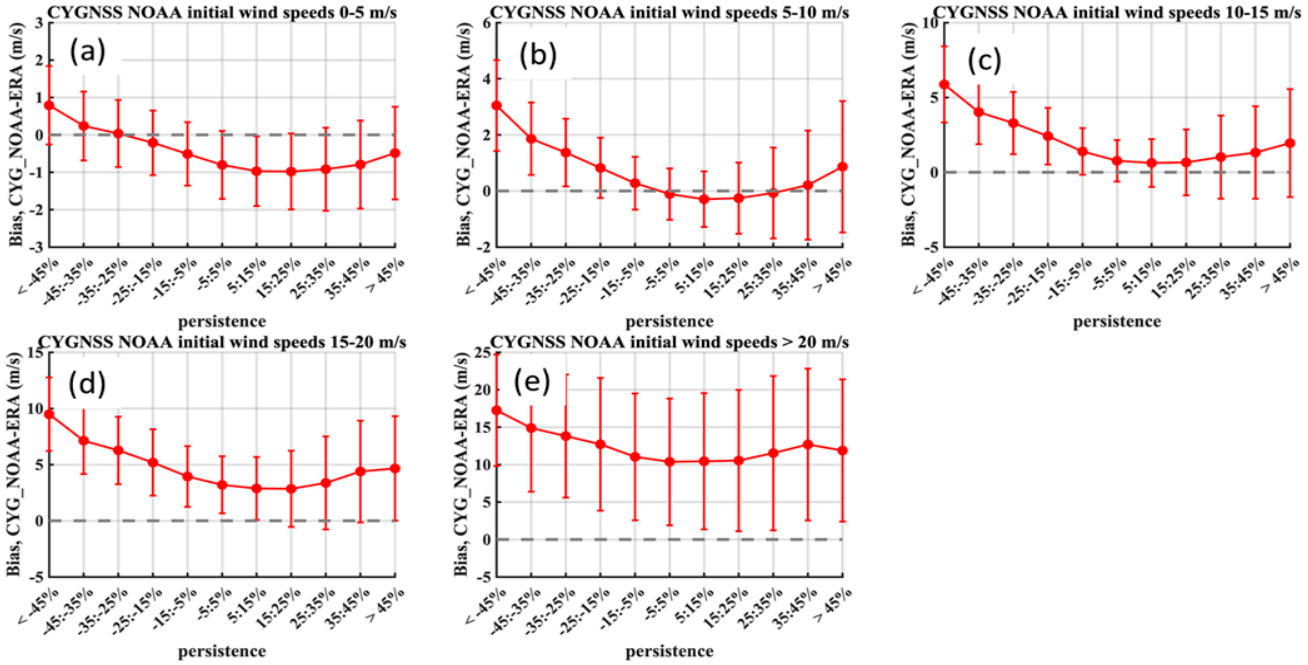

Figure 19. Bias in the CYGNSS NOAA wind speed product as a function wind speed persistence prior to the measurement for wind speed ranges of (**a**) 0–5 m/s, (**b**) 5–10 m/s, (**c**) 10–15 m/s, (**d**) 15–20 m/s, (**e**) >20 m/s. Persistence < 0 implies prior winds were higher. Bias is the average (NOAA–ERA5) difference for all of CY2022. Error bars are the standard deviation of all samples averaged in each wind speed and persistence bin.

4. Discussion of Sensitivity to Persistence

The behavior of CYGNSS wind speed retrieval bias—in particular how it varies as a function of wind speed, wind persistence, Significant Wave Height, and the approach used by the retrieval algorithm to deal with these dependencies—provides insights into the inherent sensitivity of GNSS-R measurements to portions of the ocean surface roughness spectrum not directly forced by the local wind stress. Some of these dependencies are highlighted in Table 6, which reports the bias at both typical and high wind speeds and for moderate, large negative, and large positive values of wind speed persistence. The table also reports the bias individually for the FDS and NOAA wind speed products to highlight the effects of the different retrieval algorithm approaches they use. The full range of dependencies across all wind speed and persistence values was illustrated in Figures 18 and 19.

As reported in Table 6, typical (5–10 m/s) wind speeds account for 62% of the total samples observed in all conditions. Moderate persistence values (wind speed changes over the previous 2 h of between −25% and +25% of the present wind speed) account for 95% of those samples. Under these jointly typical conditions of wind speed and persistence, the retrieval bias is very low, at 0.00 m/s for the FDS and −0.03 m/s for the NOAA product. This is to be expected since both retrieval algorithms are based on empirically derived regressions that are weighted toward the most commonly occurring conditions. For atypical persistence conditions at typical wind speeds, however, the bias can grow significantly. In the FDS case, a large negative persistence (<−25%) resulted in a bias of 2.3 m/s whereas a large positive persistence (>25%) resulted in a bias of 0.4 m/s, which is still low. The situation is similar with the NOAA product. A persistence below −25% resulted in a bias of 1.9 m/s and a persistence above 25% in a bias of 0.1 m/s. Note that the anomalously large negative persistence values only occur ~3% of the time, so they do not contribute significantly to the overall global performance statistics. A negative persistence implies that the past winds were higher than in the present. The fact that the bias is more sensitive to these conditions suggests that the retrieval algorithm is essentially tuned to expect a long wave portion of the roughness spectrum that is more consistent with lower winds.

The fact that a large positive persistence (in which case past wind speed is significantly lower than at present) does not result in a similar retrieval bias suggests that the time scale of the energy cascade from shorter to longer wavelengths of the roughness spectrum may be shorter in high wind than low wind conditions.

Table 6. Dependence of wind speed bias (CYGNSS–ERA5) on wind persistence at typical and high wind speeds.

Wind Speed Range (m/s)	**5–10 m/s**			**>20 m/s**		
% of Samples	**62%**			**0.02%**		
Persistence Range	$p < -25\%$	$p > -25$, $p < 25\%$	$p > 25\%$	$p < -25\%$	$p > -25$, $p < 25\%$	$p > 25\%$
% Samples @Wind Speed [1] (FDS/ERA5 matchup)	3.27%	94.88%	1.85%	2.93%	95.38%	1.69%
FDS—ERA5 Bias (m/s)	2.32	0.00	0.40	9.48	2.05	1.34
% Samples @Wind Speed [1] (NOAA/ERA5 matchup)	2.66%	95.81%	1.54%	4.15%	93.83%	2.02%
NOAA—ERA5 Bias (m/s)	1.92	−0.03	0.13	15.33	10.83	11.9

[1] Percentage of all ERA5 samples within the specified range of wind speed values that have the specified range of persistence values.

Table 6 also includes bias results for high wind (>20 m/s) conditions while similarly partitioning the samples into moderate, large negative, and large positive persistence. Such high winds occur infrequently (~0.02% of all samples) but the behavior of the retrieval algorithm under these conditions can nonetheless be informative. The FDS bias at moderate levels of persistence was still fairly low at 2.1 m/s, it was slightly lower (1.3 m/s) with a large positive persistence, and it had a very high bias of 9.5 m/s when there was a large negative persistence. The explanation for the high bias is similar to the lower wind speed case. A large negative persistence implies that the past wind speed was higher, in this case much higher, since the wind speed range considered was > 20 m/s. Such high winds in the past would have introduced energy into the surface roughness spectrum at smaller wavelengths that cascaded over the subsequent 1–2 h to longer waves, which would then have anomalously high amplitudes relative to an amplitude consistent with the lower wind speed in the present (when the CYGNSS measurement was made). That measurement would be of a rougher surface and have a lower scattering cross section, and hence the retrieved wind speed would be too high and thus have a positive bias observed. Again, as with the previous case at lower wind speeds, the condition of anomalously large negative persistence rarely occurs (~3% of the time), so while useful for diagnosing GNSS-R sensitivity to sea state, it is not a significant contributor to overall performance.

The behavior of the NOAA wind speed bias at high (>20 m/s) wind speeds noted in Table 6 is quite different from that of the FDS product. The bias with moderate wind speed persistence is 10.8 m/s, it grows to 11.9 m/s with large positive persistence, and grows further to 15.3 m/s with large negative persistence. The overall bias, averaged across all wind speeds, is not significantly affected because high winds happen so infrequently. The most likely cause of the large bias lies in the approach followed to create the GMF used by the NOAA wind speed retrieval algorithm. Because it was constructed empirically from a composite population of global CYGNSS and ERA5 matchups at low wind speeds and CYGNSS and HWRF matchups in storms at high wind speeds, the higher wind speed portion of its GMF has been tuned to the underdeveloped sea state conditions typical of major storms. When Fully Developed Seas at high wind speeds are encountered (which would generally be the case with moderate to low persistence values), the retrieval algorithm will tend to overestimate the wind speed. As Table 6 indicates, moderate to low

wind speed persistence tends to occur ~95% of the time, and the high NOAA retrieval bias will be present then as well as with larger values of wind speed persistence.

5. Conclusions

The performance and properties of several CYGNSS ocean surface wind speed products have been characterized in a variety of ways. The products include the Fully Developed Seas (FDS) and Merged Storm (MRG) winds produced by the project science team and an NOAA product developed independently by a research group at the NOAA Center for Satellite Applications and Research. The FDS product is intended for use globally in conditions other than major organized storms and the MRG product uses a modified retrieval algorithm applied over major storms that is then merged with the FDS product away from storms. The single NOAA product uses a common retrieval algorithm in all conditions. Performance characterization is performed in two ways. One approach compares the CYGNSS product-under-test to a reference wind speed product and assesses performance by the Root Mean Square Difference (RMSD) and mean difference (aka., the bias) between them. A second approach uses the triple colocation method to decompose the RMSD between any two wind speed products into individual estimates of the Root Mean Square Error (RMSE) in each. This approach requires coincident measurements by three independent products. The triple colocation method is advantageous when there is the possibility of significant error in a single reference wind product, in which case, the RMSD between it and the product-under-test may be significantly larger than the RMSE. This is found to be the case with performance assessment in major storms, and triple colocation is the preferred approach in that case.

The direct one-on-one comparison between CYGNSS and a reference wind product was performed using a globally distributed population of samples. Two sources for the reference equivalent-neutral winds were considered: the ERA5 reanalysis wind speed at a height of 10 m, and a large network of in situ buoy measurements that have been adjusted to a 10 m reference height. Comparisons were made with the FDS and NOAA products. The bias between CYGNSS and buoy winds was found to be 0.03 m/s and -0.22 m/s for FDS and NOAA, respectively. The RMSD between CYGNSS and buoy winds was found to be 1.36 m/s for FDS and 1.21 m/s for NOAA. The lower RMSD with NOAA is believed to result primarily from the additional spatial averaging it performs of samples that have significant overlap in their sampling footprints. This reduces the effects of noise while only slightly degrading the spatial resolution. The comparisons between CYGNSS and ERA5 showed similar behavior. The bias is -0.1 m/s and -0.03 m/s for FDS and NOAA, and the RMSD is 1.6 m/s for FDS and 1.4 m/s for NOAA. The higher RMSD values with respect to ERA5 may result at least in part from the higher uncertainty associated with ERA5 winds. This hypothesis is supported by the triple colocation results. See Sections 3.1.1 and 3.1.2 for details about the buoy and ERA5 intercomparisons.

The triple colocation method of performance assessment was applied using multiple possible triplets of coincident wind speed products for global (away from storms) winds. The consistency of the RMSE estimates between triplets is a measure of the reliability of the error decomposition it performs, and the results were indeed found to be consistent. Averaging across estimates for all possible triplets, the RMSE of the FDS product was found to be 1.35 m/s and the RMSE for the NOAA product was 0.98 m/s. These values were both lower than the RMSD values and this is likely due to the contribution to the RMSD statistic made by uncertainties in the reference wind speed product.

For performance assessment at high wind speeds in storms, the triple colocation method is also used. In this case, the availability of suitable reference wind products is more limited and a single triplet (CYGNSS, HWRF, SFMR) is used. The RMSE results are divided into different ranges of wind speed because performance was found to be a strong function of it. The RMSE of the MRG product was 3.2 m/s (wind speed < 20 m/s), 3.2–4.6 m/s (wind speed 20–30 m/s), and 4.6–6.8 m/s (wind speed 30–45 m/s). The corresponding RMSE values for the NOAA product were 4.2 m/s (wind speed < 20 m/s),

4.2–7.0 m/s (wind speed 20–30 m/s), and 7.0–8.0 m/s (wind speed 30–45 m/s). The RMSE ranges given are the high and low values over the specified range of wind speeds. The 45 m/s maximum for the wind speed range is limited by the availability of three-way coincident matchups between all the products. The RMSE can be expected to continue to rise above 45 m/s due to fundamental limitations in the sensitivity of the CYGNSS radar [43].

Triple colocation was also used to assess the performance of the 34-knot significant wind radius (R34) that is derived from the MRG wind field. R34 is a measure of storm size, and its variation with quadrant a measure of storm structure, that is frequently used by operational agencies. There are more alternate sources of R34 information because it is based on measurements in the 15–20 m/s range, and an RMSE decomposition is performed using each triplet drawn from them. Averaging over all such RMSE values, the resulting RMSE was 38 km for ASCAT, 44 km for Best Track, 49 km for SMAP, and 54 km CYGNSS MRG. While CYGNSS has the largest error, it also has a lower revisit time than the other satellite products, suggesting that it could serve as a complimentary gap filler product to better track changes on short time scales in storm size and structure. See Sections 3.2.1 and 3.2.2 for details about these triple colocation analyses.

In addition to the overall performance assessments, which are based on populations of coincident matchups that include all CYGNSS receiving satellites and all GPS transmitting satellites, and span multiple years, the bias and RMSD with respect to ERA5 were also evaluated individually for each of the two radars on each of the eight CYGNSS satellites, for each of the six versions of GPS satellites, and as a function of time from 2018 to the present. The performance was found to be consistent across all subsets of the hardware and stable over time throughout the mission lifetime.

Both the FDS and NOAA wind speed products were also evaluated with respect to their sensitivity to the Significant Wave Height (SWH) of the ocean surface at the time of the measurement. This assessment was motivated by the secondary sensitivity of GNSS-R measurements to the long wave portion of the surface roughness spectrum, in addition to its primary sensitivity to the shorter capillary waves that are more directly forced by the local wind stress. In recognition of this sensitivity, both FDS and NOAA retrieval algorithms incorporate corrections for SWH. The evaluation performed here illustrates the need for such a correction and shows that none is needed for wind speed products produced by passive microwave radiometers or scatterometer radars. It also demonstrates that the corrections implemented by the FDS and NOAA algorithms are largely successful at removing the dependence of retrieval error on SWH.

One final characterization of the behavior of the CYGSS wind speed products considered the dependence of their bias on the persistence of the wind at the location of the measurement in the 2 h prior to said measurement. In the FDS case at all wind speeds and in the NOAA case at lower wind speeds, if the winds have not changed much in the 2 h prior to a CYGNSS observation, the bias is quite low. This represents conditions in which the sea state is considered to be fully developed. If, on the other hand, the wind speed has changed significantly in the 2 h prior to a measurement, a significant bias is found to be present and that bias increases with increasing change in wind speed. This sensitivity arises because GNSS-R measurements are sensitive to both the smaller (capillary) wave portion of the roughness spectrum, which is directly influenced by the instantaneous local wind stress, as well as to longer wavelength portions of the spectrum that are excited via a time-delayed energy cascade process from shorter to longer waves that has a time scale of 1–2 h. Such rapid changes in wind speed are found to happen infrequently (~3% of the time), so the impact on overall performance statistics is low. But this bias in the presence of large changes in wind speed is nonetheless a consistent property of GNSS-R wind products. The behavior of the bias with the NOAA product at high wind speeds is distinctly different. In this case, a large bias is always present because its retrieval algorithm has been tuned to expect the underdeveloped sea state conditions found in major organized storms whenever

the wind speed is high. However, away from storms when the wind speed is high, the roughness spectrum tends to be quite different and a large retrieval bias results.

Author Contributions: Conceptualization, C.R.; methodology, C.R., M.A.-K., S.A., R.B., D.M., D.P., A.R., D.T. and A.W.; software, M.A.-K., S.A., R.B., D.M., D.P., A.R., D.T. and A.W.; validation, C.R., M.A.-K., S.A., R.B., D.M., D.P. and A.W.; formal analysis, C.R., M.A.-K., S.A., R.B., D.M., D.P. and A.W.; investigation, C.R., M.A.-K., S.A., R.B., D.M., D.P. and A.W.; resources, S.A., R.B., D.P., A.R. and D.T.; data curation, S.A., R.B., D.P., A.R. and D.T.; writing—original draft preparation, C.R., M.A.-K., S.A., R.B., D.M., D.P., D.T. and A.W.; writing—review and editing, C.R., D.P. and A.W.; visualization, M.A.-K., S.A., R.B., D.M., D.P., D.T. and A.W.; supervision, C.R.; project administration, C.R.; funding acquisition, C.R. All authors have read and agreed to the published version of the manuscript.

Funding: This research was supported in part by a NASA Science Mission Directorate contract 80LARC21DA003 with the University of Michigan.

Data Availability Statement: All CYGNSS data created or used during this study are openly available from the NASA Physical Oceanography Distributed Active Archive Center (PODAAC) at https://search.earthdata.nasa.gov/search?portal=podaac-cloud (accessed on 31 January 2024).

Conflicts of Interest: Authors Daniel Pascual was employed by the company Deimos Space UK Ltd. The remaining authors declare that the research was conducted in the absence of any commercial or financial relationships that could be construed as a potential conflict of interest.

References

1. Ruf, C.S.; Atlas, R.; Chang, P.S.; Clarizia, M.P.; Garrison, J.L.; Gleason, S.; Katzberg, S.J.; Jelenak, Z.; Johnson, J.T.; Majumdar, S.J.; et al. New Ocean Winds Satellite Mission to Probe Hurricanes and Tropical Convection. *Bull. Am. Meteorol. Soc.* **2016**, *97*, 385–395. [CrossRef]
2. Ruf, C.; Gleason, S.; McKague, D.S. Assessment of CYGNSS Wind Speed Retrieval Uncertainty. *IEEE J. Sel. Top. Appl. Earth Obs. Remote Sens.* **2018**, *12*, 87–97. [CrossRef]
3. Ruf, C.; Asharaf, S.; Balasubramaniam, R.; Gleason, S.; Lang, T.; McKague, D.; Twigg, D.; Waliser, D. In-Orbit Performance of the Constellation of CYGNSS Hurricane Satellites. *Bull. Am. Meteorol. Soc.* **2019**, *100*, 2009–2023. [CrossRef]
4. Asharaf, S.; Waliser, D.; Posselt, D.; Ruf, C.; Zhang, C.; Putra, A. CYGNSS Ocean Surface Wind Validation in the Tropics. *J. Atmos. Ocean. Technol.* **2021**, *38*, 711–724. [CrossRef]
5. Chew, C.C.; Small, E.E. Description of the UCAR/CU Soil Moisture Product. *Remote Sens.* **2020**, *12*, 1558. [CrossRef]
6. Ruf, C.S.; Chew, C.; Lang, T.; Morris, M.G.; Nave, K.; Ridley, A.; Balasubramaniam, R. A New Paradigm in Earth Environmental Monitoring with the CYGNSS Small Satellite Constellation. *Sci. Rep.* **2018**, *8*, 8782. [CrossRef]
7. Carreno Luengo, H.; Ruf, C.S. Retrieving Freeze/Thaw Surface State from CYGNSS Measurements. *IEEE Trans. Geosci. Remote Sens.* **2021**, *60*, 4302313. [CrossRef]
8. Gleason, S.; Ruf, C.S.; O'Brien, A.; McKague, D.S. The CYGNSS Level 1 Calibration Algorithm and Error Analysis Based on On-Orbit Measurements. *IEEE J. Sel. Top. Appl. Earth Obs. Remote Sens.* **2018**, *12*, 37–49. [CrossRef]
9. Clarizia, M.P.; Ruf, C.S. Wind Speed Retrieval Algorithm for the Cyclone Global Navigation Satellite System (CYGNSS) Mission. *IEEE Trans. Geosci. Remote Sens.* **2016**, *54*, 4419–4432. [CrossRef]
10. Ruf, C.S.; Balasubramaniam, R. Development of the CYGNSS Geophysical Model Function for Wind Speed. *IEEE J. Sel. Top. Appl. Earth Obs. Remote Sens.* **2019**, *12*, 66–77. [CrossRef]
11. Freilich, M.; Challenor, P. A New Approach for determining Fully Empirical Altimeter Wind Speed Model Functions. *J. Geophys. Res.* **1994**, *99*, 25051–25062. [CrossRef]
12. Clarizia, M.P.; Ruf, C.S.; Jales, P.; Gommenginger, C. Spaceborne GNSS-R Minimum Variance Wind Speed Estimator. *IEEE Trans. Geosci. Remote Sens.* **2014**, *52*, 6829–6843. [CrossRef]
13. Warnock, A.M.; Ruf, C.S.; Russel, A.; Al-Khaldi, M.M.; Balasubramaniam, R. CYGNSS Level 3 Merged Wind Speed Data Product for Storm Force and Surrounding Environmental Winds. *IEEE J. Sel. Top. Appl. Earth Obs. Remote Sens.* **2024**, *17*, 6189–6200. [CrossRef]
14. CYGNSS. *CYGNSS Level 2 Science Data Record Version 3.2*; PO.DAAC: Pasadena, CA, USA, 2024. Available online: https://podaac.jpl.nasa.gov/dataset/CYGNSS_L2_V3.2 (accessed on 31 January 2024).
15. CYGNSS. *CYGNSS Level 3 MRG Science Data Record Version 3.2.1*; PO.DAAC: Pasadena, CA, USA, 2024. Available online: https://podaac.jpl.nasa.gov/dataset/CYGNSS_L3_MRG_V3.2.1 (accessed on 31 January 2024).
16. Said, F.; Jelenak, Z.; Park, J.; Chang, P.S. The NOAA Track-Wise Wind Retrieval Algorithm and Product Assessment for CyGNSS. *IEEE Trans. Geosci. Remote Sens.* **2021**, *60*, 4202524. [CrossRef]
17. Bourles, B.; Lumpkin, R.; McPhaden, M.J. The PIRATA Program: History, Accomplishments, and Future Directions. *Bull. Am. Meteorol. Soc.* **2008**, *89*, 1111–1125. [CrossRef]

18. McPhaden, M.J.; Meyers, G.; Ando, K.; Masumoto, Y.; Murty, V.S.N.; Ravichandran, M.; Syamsudin, F.; Vialard, J.; Yu, L.; Yu, W. RAMA: The Research Moored Array for African-Asian-Australian Monsoon Analysis and Prediction. *Bull. Am. Meteorol. Soc.* **2009**, *90*, 459–480. [CrossRef]
19. McPhaden, M.J.; Busalacchi, A.J.; Cheney, R.; Donguy, J.-R.; Gage, K.S.; Halpern, D.; Ji, M.; Julian, P.; Meyers, G.; Mitchum, G.T. The Tropical Ocean-Global Atmosphere (TOGA) observing system: A decade of progress. *J. Geophys. Res.* **1998**, *103*, 14169–14240. [CrossRef]
20. Asharaf, S.; Posselt, D.J.; Said, F.; Ruf, C.S. Updates on CYGNSS Ocean Surface Wind Validation in the Tropics. *J. Atmos. Ocean. Technol.* **2022**, *40*, 37–51. [CrossRef]
21. Koschmieder, H. Methods and results of definite rain measurements. *Mon. Weather Rev.* **1934**, *62*, 5–7. [CrossRef]
22. Serra, Y.L.; A'hearn, P.; Freitag, H.P.; McPhaden, M.J. Atlas self-siphoning rain gauge error estimates. *J. Atmos. Ocean. Technol.* **2001**, *18*, 1989–2002. [CrossRef]
23. Edson, J.B.; Jampana, V.; Weller, R.A.; Bigorre, S.P.; Plueddemann, A.J.; Fairall, C.W.; Miller, S.D.; Mahrt, L.; Vickers, D.; Hersbach, H. On the Exchange of Momentum Over the Open Ocean. *J. Phys. Oceanogr.* **2013**, *43*, 1589–1610. [CrossRef]
24. Fairall, C.W.; Bradley, E.F.; Hare, J.E.; Grachev, A.A.; Edson, J.B. Bulk Parameterization of Air–Sea Fluxes: Updates and Verification for the COARE Algorithm. *J. Clim.* **2003**, *16*, 571–591. [CrossRef]
25. Liu, W.T. The effects of the variations in sea surface temperature and atmospheric stability in the estimation of average wind speed by SEASAT-SASS. *J. Phys. Oceanogr.* **1984**, *14*, 392–401. [CrossRef]
26. Boutin, J.; Etcheto, J. Seasat scatterometer versus scanning multichannel microwave radiometer wind speeds: A comparison on a global scale. *J. Geophys. Res.* **1990**, *95*, 22275–22288. [CrossRef]
27. Ricciardulli, L. Investigation of calibration changes in the ocean surface wind measurements from the TAO/TRITON buoy array. In Proceedings of the International Ocean Vector Winds Science Team Meeting (IOVWST), Salt Lake City, UT, USA, 29–31 May 2024. Available online: https://mdc.coaps.fsu.edu/scatterometry/meeting/past.php#2024 (accessed on 31 January 2024).
28. Gualtieri, G. Analysing the uncertainties of reanalysis data used for wind resource assessment: A critical review. *Renew. Sustain. Energy Rev.* **2022**, *167*, 112741. [CrossRef]
29. Murcia, J.P.; Koivisto, M.J.; Olsen, B.T.; Hahmann, A.N.; Sørensen, P.E. Validation of European-scale simulated wind speed and wind generation time series. *Appl. Energy* **2022**, *305*, 117794. [CrossRef]
30. Stoffelen, A.; Verspeek, J.A.; Vogelzang, J.; Verhoef, A. The CMOD7 Geophysical Model Function for ASCAT and ERS Wind Retrievals. *IEEE J. Sel. Appl. Earth Obs. Remote Sens.* **2018**, *10*, 2123–2134. [CrossRef]
31. Draper, D.W.; Newell, D.; Wentz, F.J.; Krimchansky, S.; Skofronick-Jackson, G.M. The Global Precipitation Measurement (GPM) Microwave Imager (GMI): Instrument overview and early on-orbit performance. *IEEE J. Sel. Top. Appl. Earth Obs. Remote Sens.* **2015**, *8*, 3452–3462. [CrossRef]
32. Klotz, B.W.; Uhlhorn, E.W. Improved stepped frequency microwave radiometer tropical cyclone surface winds in heavy precipitation. *J. Atmos. Ocean. Technol.* **2014**, *31*, 2392–2408. [CrossRef]
33. Meissner, T.; Ricciardulli, L.; Wentz, F. *Remote Sensing Systems SMAP Daily Sea Surface Winds Speeds on 0.25 Deg Grid, Version 01.0. [NRT or FINAL]*; Remote Sensing Systems: Santa Rosa, CA, USA, 2018. Available online: www.remss.com/missions/smap/ (accessed on 31 January 2024).
34. Gopalakrishnan, S.; Liu, Q.; Marchok, T.; Sheinin, D.; Tallapragada, V.; Tong, M.; Tuleya, R.; Yablonsky, R.; Zhang, X. *Hurricane Weather Research and Forecasting (HWRF) Model, Scientific Documentation—HWRF v3.4a*; Developmental Testbed Center, NOAA/AOML Hurricane Research Division: Miami, FL, USA, 2012.
35. Landsea, C.W.; Franklin, J.L. Atlantic Hurricane Database Uncertainty and Presentation of a New Database Format. *Mon. Weather Rev.* **2013**, *141*, 3576–3592. [CrossRef]
36. Zavorotny, V.U.; Voronovich, A.G. Scattering of GPS signals from the ocean with wind remote sensing application. *IEEE Trans. Geosci. Remote Sens.* **2000**, *38*, 951–964. [CrossRef]
37. Balasubramaniam, R.; Ruf, C.S. Characterization of Rain Impact on L-Band GNSS-R Ocean Surface Measurements. *Remote Sens. Environ.* **2020**, *239*, 111607. [CrossRef]
38. Gleason, S. Level 1B DDM Calibration Algorithm Theoretical Basis Document, Rev 6. In *CYGNSS Project Document 148-0137*; University of Michigan Publishing: Ann Arbor, MI, USA, 2023. Available online: https://archive.podaac.earthdata.nasa.gov/podaac-ops-cumulus-docs/cygnss/open/L1/docs/148-0137_L1B_DDM_Calibration_ATBD_R6.pdf (accessed on 31 January 2024).
39. Gleason, S.; Johnson, J.; Ruf, C.; Bussy-Virat, C. Characterizing Background Signals and Noise in Spaceborne GNSS Reflection Ocean Observations. *IEEE Geosci. Remote Sens. Lett.* **2019**, *17*, 587–591. [CrossRef]
40. Stoffelen, A. Toward the true near-surface wind speed: Error modeling and calibration using triple collocation. *J. Geophys. Res.* **1998**, *103*, 7755–7766. [CrossRef]
41. Pascual, D.; Clarizia, M.P.; Ruf, C.S. Improved CYGNSS Wind Speed Retrieval Using Significant Wave Height Correction. *Remote Sens.* **2021**, *13*, 4313. [CrossRef]

42. Chen, D.D.; Ruf, C.S.; Gleason, S.T. Response time of mean square slope to wind forcing: An empirical investigation. *J. Geophys. Res. Ocean.* **2016**, *121*, 2809–2823. [CrossRef]
43. Balasubramaniam, R.; Ruf, C.S. Development and Application of a GNSS-R Error Model for Hurricane Winds. *IEEE J. Sel. Top. Appl. Earth Obs.* **2023**, *17*, 2336–2346. [CrossRef]